

Experimental investigation on spatial phase distributions for various flow patterns and frictional pressure drop characteristics of gas liquid two-phase flow in a horizontal helically coiled rectangular tube

CAI, Bo, XIA, Guodong, CHENG, Lixin and WANG, Zhipeng

Available from Sheffield Hallam University Research Archive (SHURA) at:

<https://shura.shu.ac.uk/31095/>

This document is the Accepted Version [AM]

Citation:

CAI, Bo, XIA, Guodong, CHENG, Lixin and WANG, Zhipeng (2023). Experimental investigation on spatial phase distributions for various flow patterns and frictional pressure drop characteristics of gas liquid two-phase flow in a horizontal helically coiled rectangular tube. *Experimental Thermal and Fluid Science*, 142: 110806. [Article]

Copyright and re-use policy

See <http://shura.shu.ac.uk/information.html>

Experimental investigation on spatial phase distributions for various flow patterns and frictional pressure drop characteristics of gas liquid two-phase flow in a horizontal helically coiled rectangular tube

Bo Cai^{a,b}, Guodong Xia^{a*}, Lixin Cheng^{a,c*} and Zhipeng Wang^a

^aKey Laboratory of Enhanced Heat Transfer and Energy Conservation, Ministry of Education, Beijing University of Technology, Beijing 100124, China

^bCollege of Locomotive and Rolling Stock Engineering, Dalian JiaoTong University, Dalian 116028, China

^cDepartment of Engineering and Mathematics, Sheffield Hallam University, Howard Street, Sheffield, S1 1WB, UK

*Corresponding author: Email address: xgd@bjut.edu.cn, lixincheng@hotmail.com

Abstract

Spatial phase distributions for various flow patterns and two phase flow frictional pressure drops of air-water flow in a horizontal helically coiled rectangular tube were experimentally investigated at the liquid and gas superficial velocities of 0.11 - 2 m/s and 0.13 - 16 m/s. Local void fractions in the helically coiled tube were measured with electric conductivity probes and the corresponding flow regimes were recorded with a high-speed video camera simultaneously. The local void fractions and spatial phase distributions for various flow regimes were analyzed

according to the physical mechanisms. The spatial phase distributions of gas liquid two-phase flow in the helically coiled tube are mainly affected by the gravitational and centrifugal forces. The measured single-phase flow and two-phase flow pressure drops have been analyzed for various flow regimes. A correlation was proposed to predict the friction pressure drop of single-phase flow in the helically coiled tube. The existing gas-liquid two- phase pressure drop frictional correlations were compared to the experimental frictional pressure drop data. The Awwad et al. correlation [Int. J. Multiphase Flow, 21 (1995), 607-619] predicts 91% of the experimental data within $\pm 30\%$.

Keywords: two-phase flow, helically coiled rectangular tube, spatial phase distribution, local void fraction, friction pressure drop, electric conductivity probe, flow regime.

1. Introduction

Gas-liquid two-phase flow in helically coiled tubes is influenced by its inherent secondary flow, which can improve the performance of reactors and heat exchangers, gas-liquid mixing units and so on in engineering applications [1, 2]. The local void fraction, phase distribution and friction pressure drop characteristics of gas liquid two phase flow in helically coiled tubes is very important in understanding the behaviors and physical mechanisms of two-phase flow and heat transfer. Many studies on the void fraction and frictional pressure drops have been conducted for gas-liquid two-phase flow in helically coiled circular channels [3 - 5]. Correlations for the void fractions and two phase flow frictional pressure drops were mainly

developed for straight circular channels [6 - 8]. A variety of measurement methods such as conductivity probes, optical fiber-probes, wire mesh sensors (WMS), γ -ray tomography and so on have been developed to measure the local void fractions, phase distributions and local flow parameters [9-12]. For upward gas-liquid two-phase flow in helically coiled tubes, Zhai et al. [13], Barnea et al. [14] and Zheng and Che [15] investigated the local flow parameters of two-phase flow and indicated that the spatial phase distribution profiles always exhibit symmetric saddle shape or parabolic shape for bubbly [13, 14] and slug flow regime [15]. For gas-liquid two-phase flow in horizontal or inclined straight tubes, Wang et al. [16] and Xu et al. [17] investigated the spatial phase distributions of gas liquid two-phase flow. They found that the local void fractions near the bottom wall are smaller than those near the top wall due to the gravity effect, yet-the spatial phase distributions along the transverse cross-section direction are always symmetric. However, studies of the local void fractions and the corresponding flow regimes of gas-liquid two-phase flow in helically coiled rectangular tubes are limited.

Single phase flow in spirally coiled tubes is the fundamental to understanding the complex gas-liquid two phase flow in such tubes. A number of experimental investigations on single phase pressure drop characteristics in spirally coiled tubes have been conducted [18]. Ito [19] conducted the experiments to research the frictional pressure drop properties of single-phase flow and proposed a correlation to predicting the critical Reynolds number from laminar to turbulent flow. Manlapaz and Churchill [20] and White [21] developed the correlations for predicting the friction coefficients for single phase flow in vertical coiled tube in the laminar flow regime. Furthermore, Srinivasan et al. [22] and Ali [23] experimentally studied the friction

coefficients of single-phase flow in coiled tube for the turbulent flow regime and proposed the prediction correlations. Zhao et al. [24] performed experiments to study the effects of roughness, Reynolds number and curvature on the single phase liquid friction coefficient in coiled tubes. Other researchers experimentally investigated the characteristics of two-phase flow in helically coiled circular tubes [25, 26]. Awwad et. al [27] and Biswas and Das [28] investigated the effects of two-phase flow rate and the geometry dimensions of coiled channel on the two-phase frictional pressure drops and proposed the prediction correlations. Thandlam et al. [29] conducted the two-phase flow experiments to investigate the flow regime transition, pressure drop and holdup of gas non-Newtonian fluid in helical channels. Xia and Liu [30] and Liu et al. [31, 32] investigated the pressure drop characteristics in vertical helically coiled channel with circle cross-section or rectangular cross-section. They analyzed the effects of secondary flow on the frictional pressure drop and two-phase flow behavior.

The available studies of the local void fractions in the straight tubes have laid a foundation to understanding the void fraction distributions for other complex tubes such as helically coiled tubes but further experimental studies are needed to measure the local void fractions and the spatial phase distributions in order to understand the underlying physical mechanisms of two phase flow in such coiled tubes with non-circular shapes. In particular, the experimental investigation on intrinsic relations among the local void fractions, friction pressure drops and flow regimes in helically coiled rectangular tubes is rare. The objectives of the present study are to conduct experiments to measure the local void fractions using the state-of-the-art electric conductivity probe method, to investigate frictional pressure drop behaviors of gas-liquid two-

phase flow in the horizontal helically coiled rectangular tube corresponding to various flow regimes, analyze the spatial phase distributions in various flow regimes according to the limiting parameters involved in the gas-liquid two-phase flow in the coiled tubes and to understand the physical phenomena and mechanisms of complicated two phase phenomena in such a tube.

2. Experimental setup and measurement system

An experimental system of air-water two-phase flow was built in order to investigate the spatial phase distributions for the corresponding flow regimes and frictional pressure drops in the horizontal helically coiled rectangular tube. The spatial phase distributions and local void fractions were measured with electric conductivity probes and the corresponding flow regimes were recorded with a high-speed video camera simultaneously. The measured local void fractions and spatial phase distributions are intrinsically related to each other and the underlying physical mechanisms can be analyzed for the corresponding flow regimes.

2.1. Experimental setup and test section

Figure 1 shows the schematic diagram of the experimental setup of the air-water two phase flow in the horizontal helically coiled rectangular tube. Water is circulated into the experimental setup from a water tank with a volume of 1 m³ by a stainless-steel centrifugal pump. The flow rate of water is measured with an electromagnetic flow rate meter having an

accuracy of $\pm 0.5\%$. Air is delivered into the experimental setup from an air tank with a constant pressure of 0.8 MPa by a screw air compressor. The air tank is used to maintain a stable air flow. The volumetric flow rate of air is measured with three gas flow meters for different flow rate ranges with a maximum accuracy of $\pm 1.5\%$. Then, water and air are well mixed in a Y-connection mixer. The distance from the Y-mixer to the test section is long enough to ensure that the air-water two phase flow is fully developed before entering the test section in the experiments. The air-water mixtures flow into the test section and then flow back to the water tank which is open to the atmosphere. The water returns to the water tank while the air is vented into the atmosphere.

It is important to evaluate the entry length in the test coiled tube. However, there is limited research regarding the entry length in coiled tubes in the literature. The uniform distribution of the Taylor bubble lengths along the flow direction is an accepted method to determine the effect of entry length on two phase flow in the coiled tubes. According to our measured experimental data, the Taylor bubble length distributions are periodic over coil loops and the length distributions in the first turn are consistent with these in the second turn of the coiled channel. Therefore, the two phase flow in the coiled may be considered as fully developed flow in our experiments. The entrance of the coiled tube has little influence on the two phase flow pressure drops in the present experiments. This has also been validated by the measured single phase pressure drops in the coiled tube in the present study. This is mainly due to the full developed two phase flow before entering the coiled tube and the smooth connection of the entrance tube to the coiled tube.

Figure 2 shows the schematic diagram of the test horizontal helically coiled rectangular tube. The transparent test tube is made of plexiglass. Table 1 list the dimensions of the test coiled tube. The coil diameter D of the test coiled tube is 141 mm and the pitch P is 140 mm. The helix angle φ is 0.306 rad. The width of the cross-section of the rectangular channel is 25 mm and the height h is 34 mm.

2.2. The measurement system and methods

Measurements of the local void fractions with the electric conductivity probes and the corresponding spatial phase distributions and two-phase flow regimes with the high-speed video camera were simultaneously taken in the experiments as shown in Fig. 1. The gas and liquid phases can be indicated by using the electric conductivity probe to measure the conductivities of the two phases when the probe tip is submerged in the gas liquid two phase flow. As shown in Fig. 3 (a), the electric conductivity probe is assembled in the test coiled tube with a flange. The sealing rubber is used to stabilize the probe and prevent the leakage of fluids. The local void fractions are measured at 13 positions along the vertical line at the middle of the cross-section by moving the electric conductivity probe upward or downward at four axial locations. The distance between two measurement positions is 2 mm. Figure 3 (b) shows the geometry structure of the electric conductivity probe. The in-house electric conductivity probe was manufactured by positioning a stainless-steel needle with an outside diameter of 0.25 mm into a supporting tube with an outside diameter of 1.2 mm. The dimensions of the probe L_1 is 60 mm and L_2 is 6 mm. The needle surface except of the probe tip was electrically insulated by

an overlay of capillary insulation. A circuit of the probe supplies a DC voltage between the needles and the supporting tube. The phase discriminate passage shifted from output signals of the circuit is sampled by an A/D converter at a sampling frequency of 1 kHz. The data acquiring period of a measurement is 150 s to obtain the measured data and then store the experimental data for future reduction and analysis.

The air water two-phase pressure drop is measured with a differential pressure transducer. It has an accuracy of $\pm 0.1\%$. The measured pressure drop data are transmitted to the computer via an Agilent 34972A data acquisition instrument. The observed two-phase flow regimes and the spatial phase distributions corresponding to the flow regimes are recorded with a high-speed video camera via the backlight imaging method. The frequency range of capturing photos is from 250 to 2000 Hz and the range of shooting time is between 4.1 and 33.2 s.

3. Data reduction and uncertainty analysis of measured parameters

3.1 Data reduction method

For the spirally coiled rectangular tube, the hydraulic diameter is used in the reduction of experimental frictional pressure drop data [33, 34]. The main measurement parameters are the liquid and gas flow rates and local void fractions. With the measured gas and liquid volumetric flow rates, the superficial gas velocity U_{SG} and the superficial liquid velocity U_{SL} are calculated with the following equations, respectively:

$$U_{SG} = \frac{Q_G}{A} \quad (1)$$

$$U_{SL} = \frac{Q_L}{A} \quad (2)$$

where Q_G is the gas phase volumetric flow rate, Q_L is the liquid phase volumetric flow rate and A is the cross-section area of the test tube.

Two steps are used to measure the local void fractions and the phase distributions of two phase flow in the coiled tube. The first step is to define a phase indicator function. The second step is to obtain a time-average local void fraction. The details of these steps are as follows:

(1) The phase indicator function: The output voltage signal of the electric conductivity probe with a varying amplitude is generated due to the large difference in the conductivities of the liquid and gas phases. Figure 4 shows the raw output signal $V(t)$ of the electric conductivity probe. As the needle tip piercing and leaving the bubbles, the voltage signal falls and rises very sharply within the responding time of 3 ms. The in-house conductivity probe with a quick responding time can detect the small bubbles with a diameter of 2.5 mm in the bubbly flow regime. Therefore, it is able to measure the local void fractions under all four two phase flow regimes in the present study. The first step to normalize the output voltage of the probe is to define phase indicator function $P(t)$ as follows:

$$P(t) = \begin{cases} 0 & \text{for } V(t) \leq TV \\ 1 & \text{for } V(t) > TV \end{cases} \quad (3)$$

where t is voltage time series, TV is the threshold value applied to discriminate the gas and liquid phases. The threshold value (TV) is crucial to define the phase indicator function and determine the local void fractions. Comparative experiments using the flow visualization method and the electric conductivity probe were conducted to determine the TV value and validate the performance of the probe. Figure 5 shows the comparative results of the two methods to measuring the resident times for Taylor bubbles and the liquid slugs. It shows that the slug units measured with the electric conductivity probe favorably agree to the measured results with the flow visualization method when the TV value is $0.75 \cdot \text{MAX}[V(t)]$. The error between the two measurement results using the two methods to measuring the resident times of slug units is less than $\pm 7.6\%$.

(2) The time-average local void fraction: As the bubbles flow through the probe, the resident time of the gas phase across the needle tip can be acquired from the phase indicator function $P(t)$. The time-averaged local void fraction α_y at a given vertical and axial position in the cross-section at a sampling time T is calculated as follows:

$$\alpha_y = \frac{1}{T} \sum_{i=1}^n \Delta T_i \quad (4)$$

where y is the vertical coordinate in the cross-section of the rectangular coiled tube, ΔT_i is the resident time of the i th bubble, n is the sampling number of bubbles.

3.2 Experimental conditions and measurement uncertainties

Experiments of air-water two-phase flow were conducted at 20°C. Table 2 lists the experimental conditions. The superficial liquid velocity varies from 0.11 to 2 m/s and the superficial gas velocity varies from 0.13 to 16 m/s. The local void fractions were measured corresponding to the flow regimes simultaneously recorded with the high-speed video camera.

The methods of Taylor [35] were used to analyze the measurement uncertainties. Table 3 lists the uncertainties of measurement parameters. The uncertainties of the coiled tube width and height are $\pm 1.47\%$ and $\pm 2\%$, respectively. The uncertainty of channel cross-section area is $\pm 3.47\%$. The uncertainties of the gas and liquid volumetric flow rates are $\pm 0.5\%$ and $\pm 1.5\%$, respectively. The uncertainty of the liquid phase superficial velocity is $\pm 4.97\%$ and the uncertainty of the gas phase superficial velocity is $\pm 3.97\%$. The uncertainty of time-averaged local void fraction is $\pm 8.65\%$.

4 Experimental results and analysis

In this section, the experimental results of local void fractions and phase distributions for the observed flow regimes, single phase and two phase frictional pressure drops are presented and discussed. The physical phenomena and mechanisms are analyzed. Several correlations for single phase and two phase frictional pressure drops are evaluated with the experimental data.

4.1 The local void fraction profiles for four flow regimes in the helically coiled rectangular tube

Four main flow regimes are identified in the horizontal helically coiled rectangular tube: severe slugging flow, bubbly flow, intermittent flow regime and annular flow [36, 37]. The measured local void fractions and spatial phase distributions at the axial position θ of 540° for the four flow regimes are presented and discussed here.

4.1.1 The local void fraction profiles in the severe slugging flow regime

The severe slugging flow regime is a type of discontinued two-phase flow at low liquid and gas flow rates. The liquid phase initially accumulates at the bottom of the coiled rectangular tube at the low gas flow rates. Then, the liquid phase increases at the entrance, forms severe liquid slug and causes the increase of the pressure drop in the coiled tube. Once the accumulated liquid slug reaches certain amount, it rapidly flows away and a new cycle will start again. This phenomenon is called severe slugging flow. Figures 6 and 7 show the measured local void fraction profiles in the severe slugging flow at the axial position of 540° for two different experimental conditions. Figure 6 shows the local void fraction distributions at a constant superficial liquid velocity of 0.131 m/s and three different superficial gas velocities of 0.825, 1.307 and 2.026 m/s. With increasing the superficial gas velocity, the local void fraction profile becomes flat and the local void fraction increases. Figure 7 shows the local void fraction distributions at a constant superficial gas velocity of 0.85 m/s and three different superficial

liquid velocities of 0.113, 0.245 and 0.358 m/s. With increasing the superficial liquid velocity, the local void fraction curves become steep and the local void fraction significantly decreases. The maximum values on the curves always appear near the outer wall of the coiled rectangular tube. The severe slugging flow is mainly dominated by the gravity.

4.1.2 The local void fraction profiles in the bubbly flow regime

The effects of the superficial liquid and gas velocities on the spatial phase distributions and the physical mechanisms in the bubbly flow regime are analyzed here. Figure 8 shows the local void fraction distributions at a constant superficial liquid velocity of 1.209 m/s and three different superficial gas velocities of 0.327, 0.49 and 0.817 m/s. With increasing the superficial gas velocity, the local void fraction profiles become steep and the local void fractions increase. Figure 9 shows the local void fraction distributions at a constant superficial gas velocity of 0.327 m/s and three different superficial liquid velocities of 1.013, 1.095 and 1.209 m/s. With increasing the superficial liquid velocity, the local void fraction distribution profiles reach peaks and the maximum values are shifted to the inner wall of the coiled rectangular tube.

Figure 10 shows the images of different flow regimes at various superficial gas and liquid velocities. As shown in Fig. 10(a)-(f), more bubbles move to the inner wall of the coiled tube while the liquid phase is shifted to the outer wall of the coiled tube at higher liquid flow rates. It indicates that the higher liquid flow rate the stronger centrifugal force affecting on the spatial phase distributions in the bubbly flow regime.

4.1.3 The local void fraction profiles in the intermittent flow regime

The effects of superficial liquid and gas velocities on the spatial phase distributions and physical mechanisms in the intermittent flow regime are analyzed here. Figure 11 shows the local void fraction distributions at a constant superficial liquid velocity of 0.605 m/s and three different superficial gas velocities of 0.49, 1.209 and 2.026 m/s. The void fraction profiles in the intermittent flow regime are unsymmetrical and the parabolic curves. With increasing the superficial gas velocity, the local void fractions increase and the peak values on the curves move to the inner wall region of the coiled rectangular tube. However, at superficial gas velocity of 2.026 m/s, the local void fraction decreases in the outer wall region of the coiled tube. As shown in the images in Fig. 10(g)-(i), with increasing the superficial gas velocity from 1.209 to 2.026 m/s, Taylor bubbles get closer to the inner wall of the coiled tube and the liquid phase is shifted to the outer side of the coiled tube. Higher superficial gas velocities may cause strong secondary flow and strong liquid turbulence, which induce more liquid phase to shift to the outer wall of the coiled tube. Figure 12 shows the local void fraction distributions at a constant superficial gas velocity of 1.961 m/s and three different superficial liquid velocities of 0.533, 0.654 and 0.83 m/s. With increasing the superficial liquid velocity, the local void fraction in the outer wall region of the tube decreases while it increases in the inner wall region of the tube. The local void fraction profiles become peak and the maximum values on the curves shift to the inner wall of the coiled tube. As shown in Figs. 10(j)-(l), at a low superficial liquid velocity of 0.533 m/s, the flow is mainly dominated by the gravity force, which results in the

liquid film on the inner wall thicker than that on the outer wall. However, with the superficial liquid velocity increasing to 0.83 m/s, the liquid film on the outer wall is thicker than that on the inner wall due to the effect of the centrifugal force overcoming the gravity effect. In this case, the local void fraction distributions in the intermittent flow regime are affected by both the gravity and the centrifugal force.

4.1.4 The local void fraction profiles in the annular flow regime

The effects of the superficial liquid and gas velocities on the spatial phase distributions and physical mechanisms in the annular flow regime are analyzed here. Figure 13 shows the local void fraction distributions at a constant superficial liquid velocity of 0.165 m/s and three different superficial gas velocities of 7.327, 9.203 and 11.11 m/s. The local void fraction in the annular flow regime slightly increases with increasing the superficial gas velocity. As shown in Fig. 10(m)-(o), with increasing the superficial gas flow velocity, the liquid film thickness on the outer wall of the coiled tube decreases and the gas-liquid interface becomes less wavy due to the increase of the shear stress on the gas-liquid interface. Figure 14 shows the local void fraction distributions at a constant superficial gas velocity of 9.15 m/s and three different superficial liquid velocities of 0.165, 0.425 and 0.67 m/s. The maximum values of the profiles are approximately 1 because the measurement positions are in the gas core. At higher superficial liquid velocity, the local void fractions near the outer wall region rapidly decrease. This indicates the liquid film thick on the outer of channel is largely influenced by the superficial liquid velocity. The liquid film thickness in the annular flow regime is mainly

affected by the centrifugal force. Such an effect becomes strong at high superficial liquid velocities.

4.2. Evolution of the local void fraction profiles along the flow direction

The local void fractions and spatial phase distribution profiles in the helically coiled rectangular tubes are mainly influenced by the combined centrifugal force, gravity force and buoyancy force [31]. Figure 15 shows the measured local void fraction distributions at four different axial locations of 360°, 450°, 540° and 630° for the superficial liquid velocities of 0.6 m/s and 0.8 m/s. It shows that the peak values are close to the inner wall of the coiled tube at the axial locations of 360°, 450°, 540° and 630° due to the centrifugal acceleration. At the axial location of 360°, the local void fraction profiles become steep and the peak values are higher as compared to those at other two axial positions of 450° and 540°. This is because more liquid phase is distributed near the outer wall of the coiled tube due to the combined effect of the centrifugal force and gravity. At the axial location of 540°, the peak values on the profiles are close to the center of the coiled tube because the centrifugal force effect is partly offset by the gravity. As shown in Figs. 15(a) and (b), the peak values on the curves are closer to the inner wall for all four measurement positions at the superficial liquid velocity of 0.8 m/s than these as the superficial liquid velocity of 0.6 m/s. It indicates that the phase distributions are significantly affected by the centrifugal force in any position of the coiled rectangular tube.

4.3. Experimental results of single phase frictional pressure drops in the coiled tube

The total experimental pressure drops of single-phase flow in the helically coiled tube ΔP_{Exp} is the sum of the frictional pressure drop ΔP_f , the acceleration pressure drop ΔP_a , and the gravitational pressure drop ΔP_g as:

$$\Delta P_{\text{Exp}} = \Delta P_g + \Delta P_a + \Delta P_f \quad (5)$$

The average measured single phase flow pressure drop is as follows:

$$\Delta P_{\text{Exp}} = \Delta P_f \quad (6)$$

The experimental single-phase flow friction coefficient λ_L the helically coiled channel is calculated as follows:

$$\lambda_L = \frac{2\Delta P_f d_h}{\rho_L U_{SL}^2 L} \quad (7)$$

where, L is the length of spiral channel which is expressed by the following equation:

$$L = N_c \sqrt{(\pi D)^2 + P^2} \quad (8)$$

where, N_c is the number of turns of the coiled tube.

Figure 16 shows the variation of the experimental friction factors λ_L with Reynolds number Re_L in the laminar and turbulent flow regimes. The critical transition Reynolds number Re_{cr} from laminar to turbulent flow in the coiled tube is determined by the correlation proposed by Ito [18]. In Fig. 16, the measured friction factors λ_L are also compared to the available correlations listed in Table 4. It should be realized that these correlations are applicable to vertical coiled tubes with circular cross-section. It can be seen that the experimental friction factor λ_L sharply decreases with increasing the Reynolds number Re_L in the laminar flow regime while it slowly decreases in the turbulent flow regime. The experimental friction factors favorably agree with the calculated friction factors with the correlation proposed by Ali [23] but higher than those calculated by other correlations in the turbulent flow regime. The experimental friction factors λ_L are bigger than the predicted values by all the correlations in the laminar flow regime.

All the correlations used in the comparison are for circular tubes while the cross section of the tube in the present study is rectangular. Therefore, care must be taken for the comparative results. First, an entry length (non-fully developed condition) exists at the inlet although it is ignored in the present study as described in the afore-going. Therefore, it is recommended that the effect of non-fully developed entrance flow on the pressure drop should be focused on in future. Second, the concept of hydraulic diameter is used in most pressure drop calculation methods. It is known that this concept doesn't work well for laminar flows and the errors could be up to 40% while it works better for turbulent flows and the errors could only be up to 15%. This is in agree to the comparative results in the present study. Although turbulent flow is

mostly used in industrial practice, careful experiments and new concepts in dealing with laminar flow in both circular and non-circular tubes should be taken care in future.

Based on the Manlapaz and Churchill [20] correlation for both laminar and turbulent flow regimes, a new correlation has been proposed by considering the effect of geometry structure as:

$$\left\{ \begin{array}{l} \text{For laminar flow} \\ \text{For turbulent flow} \end{array} \right. \quad \frac{\lambda}{\lambda_s} = \lambda_b \left[1 + \left(1 + \frac{d_h}{D} \right)^2 \left(\frac{Dn}{88.33} \right) \right]^{2.5}, \lambda_s = 64/Re \text{ and } \lambda_b = 1.142$$

$$\lambda = 0.18Re^{-1/8} (d_h/D_{eq})^{0.15}, D_{eq} = \sqrt{P^2 + (\pi D)^2} / \pi \quad (9)$$

Figure 17 shows the comparative results between the experimental friction factors of single-phase flow and calculated friction factors with the new proposed correlation. The new proposed correlation favorably predicts all the experimental friction factors within $\pm 10\%$. The proposed correlation should be further validated/improved with large experimental data at a wide range of conditions in the laminar and turbulent flow and the consideration of the entry length effect in future.

4.4. Experimental results of gas liquid two phase frictional pressure drop in the coiled tube

For adiabatic two phase flow in the horizontal coiled tube, the gravitational and

acceleration pressure drops can be neglected, the average experimental two-phase pressure drop $\Delta P_{TP,Exp}$ is equal friction two-phase pressure drop $\Delta P_{TP,f}$ as follows:

$$\Delta P_{TP,Exp} = \Delta P_{TP,f} \quad (10)$$

The average two phase pressure drop gradient in the coiled rectangular tube is as

$$\left(\frac{dP}{dL}\right)_{TP} = \frac{\Delta P_{TP,Exp}}{N_c[(\pi D)^2 + P^2]} \quad (11)$$

According to the Lockhart-Martinelli (L-M) [6] two phase flow separate phase model, the multiplier friction coefficients of the liquid phase Φ_L^2 and the gas phase Φ_G^2 are expressed as follows:

$$\Phi_L^2 = \frac{\left(\frac{dP}{dL}\right)_{TP}}{\left(\frac{dP}{dL}\right)_L} \quad (12)$$

$$\Phi_G^2 = \frac{\left(\frac{dP}{dL}\right)_{TP}}{\left(\frac{dP}{dL}\right)_G} \quad (13)$$

The L-M parameter X is defined as

$$X^2 = \frac{\left(\frac{dP}{dL}\right)_L}{\left(\frac{dP}{dL}\right)_G} \quad (14)$$

where $(dP/dL)_L$ and $(dP/dL)_G$ are the frictional pressure gradients for single liquid phase flow and single gas phase flow, which are expressed as follows:

$$\left(\frac{dP}{dL}\right)_L = \lambda_L \frac{1}{d_h} \frac{\rho_L U_{SL}^2}{2} \quad (15)$$

$$\left(\frac{dP}{dL}\right)_G = \lambda_G \frac{1}{d_h} \frac{\rho_G U_{SG}^2}{2} \quad (16)$$

where, λ_L and λ_G are the friction factors of single liquid phase flow and single gas phase flow, respectively.

Chisholm [7] proposed a correction for the two phase flow multiplier friction factors according to the L-M curve as

$$\Phi_L^2 = 1 + \frac{C}{X} + \frac{1}{X^2} \quad (17)$$

where C is dimensionless parameter determined by the flow regime of single-phase flow as shown in Table 5.

It must be mentioned here that in the one-dimensional expression given in Eq. (10), the experimental pressure drop is strictly not the frictional pressure drop. The reason is that the acceleration pressure drop is not strictly zero as the void fraction at the inlet (not a fully developed condition for the coiled tube) is not the same as that at the outlet. The acceleration pressure drop decreases as the pipeline length where the pressure drop is measured increases.

The entry length is small as compared to the total length. The acceleration pressure drop is ignored [27]. This is also due to the adiabatic two phase flow condition. In the present study, the experimental pressure drop is taken as frictional pressure drop in the following analysis and discussion. However, it is recommended that the effect of non-fully developed entrance flow on the frictional pressure drop should be investigated in future.

The effects of the superficial gas and liquid velocities and flow regimes on the measured two phase frictional pressure drops are analyzed here. Figure 18(a) shows the experimental two phase frictional pressure drops at lower superficial gas velocities and figure 18(b) shows the experimental two phase frictional pressure drops at higher superficial gas velocities. As shown in Fig. 18(a), the two phase frictional pressure drops firstly slowly increase and then rapidly decreases and finally increase with increasing the superficial liquid velocity. This is because the flow regime transition from the severe slugging flow to the bubbly and intermittent flows, which results in a sudden decrease of the two phase frictional pressure drop in the coiled rectangular tube. As shown in Fig. 18(b), the two phase frictional pressure drops increase with increasing the superficial liquid and gas velocities in the intermittent flow and annular flow regimes.

Figure 19 shows the effect of flow regimes on the two phase frictional pressure gradients. It shows that the the two-phase frictional pressure gradients increase with increasing the superficial gas and liquid velocities in the bubbly, intermittent and annular flow regimes. However, in the severe slugging flow regime, the two phase frictional pressure gradients decrease with increasing the superficial gas and liquid flow velocities. This is because the

backflow occurs in the severe slugging flow regime while it becomes weakened with increasing the superficial gas and liquid velocities.

The Lockhart-Martinelli (L-M) [6] correlation is one of the most popular correlations for predicting the two phase flow frictional pressure drops in straight tubes. The experimental two phase multiplier friction coefficients are compared to the calculated two phase multiplier friction coefficients with Eq. (17). Figure 20 shows the comparative results between the experimental two phase multiplier friction coefficients and the calculated results with the L-M correlation. The two-phase multiplier friction coefficients for straight pipes calculated by the L-M correlation for $C = 5, 12, \text{ and } 20$ are also presented in Figure 20. It is obvious that the calculated two phase multiplier friction coefficients are lower than the calculated results in the helically coiled tube at low gas and liquid Reynolds numbers. On the one hand, the backflow caused by the gravity in severe slugging flow regime leads to higher friction pressure drops in the coiled tube than these in a straight tube. On the other hand, the centrifugal force of the liquid phase in the coiled tube results in increase of frictional pressure drops on the outer wall of the coiled tube. Therefore, the L-M correlation underpredicts the experimental two-phase multiplier friction coefficients in the coiled rectangular tubes because of the effects of gravity and the centrifugal force.

Awad et al. [27] developed a correlation of the liquid phase multiplier for predicting the two-phase pressure drop in the coiled tubes with circular cross-section by considering the gravity and centrifugal force effects. They introduced the liquid Froude number Fr_L and the proportion of the hydraulic diameter to the pitch diameter d_h/D . The dimensionless number Fr_L

represents the effect of the ratio of the inertial force and the gravity on the two phase frictional pressure drop and the dimensionless parameter d_h/D represents the effect of centrifugal force on the two phase frictional pressure drop. The Awwad et al. correlation is as follows:

$$\Phi_L = \left[1 + \frac{X}{C_0[F_d]^m} \right] \left(1 + \frac{12}{X} + \frac{1}{X^2} \right)^{\frac{1}{2}} \quad (18)$$

$$F_d = Fr_L^2 \delta^{0.1} = \frac{U_{SL}^2}{g d_h} \left(\frac{d_h}{D} \right)^{0.1} \quad (19)$$

where Fr_L is the liquid phase Froude number and δ is the curvature of channel. If $F_d \leq 0.3$, then $C_0 = 7.79$, $m = 0.576$ and if $F_d \geq 0.3$, $C_0 = 13.56$, $m = 1.3$.

Figure 21 shows the comparative results between the experimental two phase multiplier friction coefficients and the predicted results with the Awwad et al. correlation. The Awwad et al. correlation predicts 91% of experimental data within $\pm 30\%$. This is reasonably good for the complicated gas liquid two phase flow in coiled rectangular tubes. Therefore, the Awwad et al. correlation is applicable to the experimental data in the coiled rectangular tube under a wide range of experimental conditions in the present study. Furthermore, it shows that the two-phase frictional pressure drops are mainly affected by the helically coiled structures while it is less affected by the cross-section geometry of the helically coiled tubes.

5. Conclusions

Experiments of the local void fractions, spatial phase distributions, flow regime observations, single phase and two phase frictional pressure drops in the helically coiled rectangular tube were simultaneously conducted at a wide range of the liquid superficial velocities from 0.11 to 2 m/s and the gas superficial velocities from 0.13 to 16 m/s. The physical mechanisms for the local void fractions and spatial phase distributions for the four observed flow regimes are analyzed. The single phase and two phase frictional pressure drops are compared to the available correlations in the literature. The following conclusions have been obtained:

(1) One distinguishing feature of the local void fraction phase distributions for the helically coiled rectangular tube is unsymmetrical distributions. The flow regimes, the superficial gas and liquid velocities have a significant effect on the local void fractions and the phase distributions.

(2) Due to the dominating effect of the gravity, the local void fractions and spatial phase profiles in the severe slugging flow regime show sharp peak distributions near the outer wall of the coiled rectangular tube.

(3) The bubbly flow regime occurs at high superficial liquid velocities which cause high liquid turbulence in the two phase flow. The local void fractions and spatial phase distribution profiles in the bubbly flow regime show a shape of peak distribution near the inner wall of the coiled rectangular tube due to the dominating effect of the centrifugal force.

(4) The local void fractions and the spatial phase distribution profiles in the intermittent

and annular flow regimes show either shape peak distributions in the central of the coiled rectangular tube or shape peak distributions near the inner wall of the tube at different superficial gas and liquid velocities.

(5) With increasing the superficial gas velocity, the local void fractions in all flow regimes increase expect for those in the intermittent flow regimes. At higher superficial gas phase velocities, the local void fractions near the outer wall region decrease. This indicates that increasing the superficial gas velocity makes more liquid phase shift to the outer wall of the coiled rectangular tube. With increasing the superficial liquid velocity, the local void fractions near the outer wall region in all other flow regimes decrease expect for those in the severe slugging flow regime due to the dominating centrifugal force effect in these flow regimes. Due to the effect of the centrifugal force generated in the coiled rectangular tube, the liquid film thicknesses on the outer side rectangular tube wall in the bubbly, intermittent and annular flow regimes increase with increasing the superficial liquid velocity.

(6) The two phase frictional pressure drops increase with increasing the superficial gas and liquid velocities in the bubbly, intermittent and annular flow regimes. However, the two-phase fraction pressure drops decrease in the severe slugging flow regime with increasing the superficial gas and liquid velocities because the backflow occurs in this flow regime.

(7) A new correlation for predicting single phase friction pressure drop in the helically rectangular coiled tube has been developed. It favorably predicts all the experimental friction factors within $\pm 10\%$ in the present study. The two phase frictional pressure drops in helically coiled rectangular tube are higher than these in straight tubes at low superficial gas and liquid

flow velocities because of the effects of the gravity and the centrifugal force. The two phase frictional pressure drops in the coiled rectangular tube are mainly affected by the helically coiled structures while they are less affected by the cross-section geometry. The Awwad et al. correlation favorably predicts 91% of the experimental two phase multiplier friction coefficients within $\pm 30\%$.

Nomenclature

A	Area of rectangular cross-section, m^2
C	dimensionless parameter
C_0	coefficient in equation (17)
D	coil diameter, m
D_{eq}	equal coil diameter, m
Dn	Dean number
d_h	hydraulic diameter of coiled channel, m
F_d	the coefficient in equation (19)
Fr	Froude number
f_b	buoyance force, N
f_c	centrifugal force, N

f_g	gravity force, N
g	gravity acceleration, m/s ²
h	height of rectangular cross-section of channel, m
L	length of coiled channel, m
L_1, L_2	geometric parameter of probe, m
$L-M$	Lockhartd-Martinelli
ll	laminar-laminar
lt	laminar-turbulent
m	coefficient in equation (18)
N_c	number of turns of the coiled channel
n	sampling size of bubbles
P	pitch, m
$P(t)$	phase discriminate function
Q_G	gas phase volumetric flow rate, m ³ /s
Q_L	liquid phase volumetric flow rate, m ³ /s
Re	Reynolds number
Re_{cr}	critical Reynolds number from laminar to turbulent flow

Re_L	liquid phase Reynolds number
T	sampling time, s
TV	threshold value
t	voltage time series, s
tl	turbulent-laminar
tt	turbulent-turbulent
U_{SG}	superficial gas velocity, m/s
U_{SL}	superficial liquid velocity, m/s
$V(t)$	output voltage signal of the probe, V
w	width of rectangular cross-section of channel, m
X	Lockhart-Martinelli number
x	horizontal axis from measurement position to the side wall, m
y	vertical axis from measurement position to the bottom wall, m

Greeks

α_y	time-averaged local void fraction
ΔP_a	accelerated pressure drop of single-phase flow, Pa

ΔP_f	frictional pressure drop of single-phase flow, Pa
ΔP_g	gravity pressure drop of single-phase flow, Pa
ΔP_{Exp}	total experimental pressure drop of single-phase flow, Pa
$\Delta P_{TP,f}$	friction pressure drop of two-phase flow, Pa
$\Delta P_{TP,Exp}$	total experimental two-phase pressure drop, Pa
ΔT_i	resident time of i th bubble, s
δ	curvature of coiled channel
θ	axial position along helically channel, °
λ	Darcy friction coefficient
λ_b	the coefficient in equation (9)
λ_G	Darcy friction coefficient of gas phase
λ_L	Darcy friction coefficient of liquid phase
λ_s	Darcy friction coefficient of vertical flow
ρ_L	liquid density, kg/m ³
ρ_G	gas density, kg/m ³
σ	surface tension, N/s
Φ_L^2	multiplier friction coefficient of liquid phase

Φ_G^2 multiplier friction coefficient of gas phase

φ helix angle, rad

Subscripts

a acceleration

c coil

Exp experimental

eq equivalent

f frictional

G gas

g gravitational

h hydraulic

i i th

L liquid

Pre predicted

SG superficial gas

SL superficial liquid

TP two phase

y y-axis

References

- [1] S.P. Oliviera, J.P. Meyera, M.D. Paepe, K.D. Kerpel, The influence of inclination angle on void fraction and heat transfer during condensation inside a smooth tube, *Int. J. Multiphase Flow*. 80 (2016) 1-14. <https://doi.org/10.1016/j.ijmultiphaseflow.2015.10.015>.
- [2] J.A. Millcie, S. Garimella, M.P. Macdonald, Flow regimes and void fractions during condensation of hydrocarbons in horizontal smooth tubes, *Int. J. Heat and Mass Trans.* 92 (2016) 252-267. <https://doi.org/10.1016/j.ijheatmasstransfer.2015.08.017>.
- [3] R. Srisomba, O. Mahian, A.S. Dalkilic, S. Wongwises, Measurement of the void fraction of R-134a flowing through a horizontal tube, *Int. Comm. Heat Mass*. 56 (2014) 8-14. <https://doi.org/10.1016/j.icheatmasstransfer.2014.04.004>.
- [4] M. Lolcanathan, T. Hibiki, Flow regime, void fraction and interfacial area transport and characteristics of co-current downward two-phase flow, *Nuclear Eng. Des.* 307 (2016) 39-63. <https://doi.org/10.1016/j.nucengdes.2016.05.042>.
- [5] L. Cheng, G. Ribatski, J.R. Thome, Two-Phase Flow Patterns and Flow-Pattern Maps: Fundamentals and Applications, *Appl. Mech. Rev.* 61 (2008) 050802. <https://doi.org/10.1115/1.2955990>
- [6] R.W. Lockhart, R.G. Martinelli, Proposed correlations for isothermal two-phase two-

- component flow in pipes, *Che. Eng. Prog.*, 8 (1949) 39-48.
- [7] D. Chisholm, A theoretical basis for the Lockhart–Martinelli correlation for two-phase flow, *Int. J. Heat and Mass Trans.*, 10 (1967) 1767–1778. [https://doi.org/10.1016/0017-9310\(67\)90047-6](https://doi.org/10.1016/0017-9310(67)90047-6).
- [8] Y.Q. Xue, H.X. Li, C.Y. Hao, C. Yao, Investigation on the void fraction of gas-liquid two-phase flows in vertically-downward pipes, *Int. Comm. Heat and Mass.*, 77 (2016) 1-8. <https://doi.org/10.1016/j.icheatmasstransfer.2016.06.009>.
- [9] R.E. Vieira, M. Parsi, B.S. McLaury, et. al, Experimental characterization of vertical downward two-phase annular flows using Wire-Mesh Sensor, *Chem. Eng. Sci.* 134 (2015) 324-339. <https://doi.org/10.1016/j.ces.2015.05.013>.
- [10] X.Z. Shen, K. Mishima, H. Nakamura, Error reduction, evaluation and correction for the intrusive optical four-sensor probe measurement in multi-dimensional two-phase flow, *Int. J. Heat Mass Trans.* 51 (2008) 882–895. <https://doi.org/10.1016/j.ijheatmasstransfer.2006.01.054>
- [11] J. Enrique Juliá, W.K. Harteveld, R.F. Mudde, H.E. Van den Akker, On the accuracy of the void fraction measurements using optical probes in bubbly flows, *Rev. Sci. Instrum.* 76 (2005) 035103. <https://doi.org/10.1063/1.1862192>.
- [12] J. Xue, M. Al-Dahhan, M.P.P. Dudukovic, R.F.F. Mudde, Four-point optical probe for measurement of bubble dynamics: validation of the technique. *Flow Meas, Instrum.* 19 (2008) 293–300. <https://doi.org/10.1016/j.flowmeasinst.2007.10.004>.

- [13] L.S. Zhai, P. Bian, Z.K. Gao, N.D. Jin, The measurement of local flow parameters for gas-liquid two-phase bubbly flows using a dual-sensor probe array, *Chem. Eng. Sci.* 144 (2016) 346-363. <https://doi.org/10.1016/j.ces.2016.01.058>.
- [14] D. Barnea, E. Roitberg, L. Shemer, Spatial distribution of void fraction in the liquid slug in the whole range of pipe inclinations, *Int. J. Multiphase Flow.* 52 (2013) 92-101. <https://doi.org/10.1016/j.ijmultiphaseflow.2012.12.005>.
- [15] D.H. Zheng, D.F. Che. Experimental study on hydrodynamic characteristics of upward gas-liquid slug flow, *Inter. J. Multiphase Flow.* 32 (2006) 1191-1218. <https://doi.org/10.1016/j.ijmultiphaseflow.2006.05.012>.
- [16] X. Wang, T.J. Wang, L.M. He, Measurement of gas entrainment from stationary liquid slug in horizontal tube with double-sensor conductivity probe, *Flow Meas. Instrum.* 27 (2012) 81-91. <https://doi.org/10.1016/j.flowmeasinst.2012.07.002>.
- [17] L.J. Xu, W.F. Xu, Z. Cao, X.B. Liu, J.H. Hu, Multiple parameters' estimation in horizontal well logging using a conductance-probe array, *Flow. Meas. Instrum.* 40 (2014) 192–198. <https://doi.org/10.1016/j.flowmeasinst.2014.05.021>.
- [18] H. Itō, Laminar Flow in Curved Pipes, *J. Appl. Math. Mech.* 49(1969) 653. <https://doi.org/10.1002/zamm.19690491104>.
- [19] H. Ito, Friction factors for turbulent flow in curved pipes, *J. Basic Eng.* 81(1959) 123-134. <https://doi.org/10.1115/1.4008390>.

- [20] R.L. Manlapaz, S.W. Churchill, Fully developed laminar flow in a helically coiled tube of finite pitch, *Chem. Eng. Comm.* 7(1980) 57-78.
<https://doi.org/10.1080/00986448008912549>
- [21] C.M. White, Streamline Flow through curved pipes, *Proc. Roy. Soc. (London)*, A123 (1929) 645. 10.2307/95217.
- [22] P.S. Srinivasan, S.S. Nandapur, F.A. Holland, Pressure drop and heat transfer in coils, *Tran. Institution Chem. Eng.* 46 (1968) 113-119.
- [23] S. Ali, Pressure drop correlations for flow through regular helical coil tubes, *Fluid Dyn. Res.* 28 (2001) 295-310. [https://doi.org/10.1016/S0169-5983\(00\)00034-4](https://doi.org/10.1016/S0169-5983(00)00034-4).
- [24] H. Zhao, X. Li, X. Wu. New friction factor equations developed for turbulent flows in rough helical tubes, *Int. J. Heat Mass Tran.* 95 (2016) 525-534.
<https://doi.org/10.1016/j.ijheatmasstransfer.2015.12.035>
- [25] M. Mozafari, M.A. Akhavan-Behabadi, H. Qobadi-Arfaee, et al. Condensation and pressure drop characteristics of R600a in a helical tube-in-tube heat exchanger at different inclination angles, *Appl. Therm. Eng.* 90 (2015) 571-578.
<https://doi.org/10.1016/j.applthermaleng.2015.07.044>.
- [26] R. Dong, F. Niu, Y. Zhou, et al. Modeling analyses of two-phase flow instabilities for straight and helical tubes in nuclear power plants, *Nucl. Eng. Des.* 307 (2016) 205-217.
<https://doi.org/10.1016/j.nucengdes.2016.07.001>.
- [27] A. Awwad, R.C. Xin, Z.F. Dong, et al. Measurement and correlation of the pressure drop

- in air-water two-phase flow in horizontal helicoidal pipes, *Int. J. Multiphase Flow.* 21 (1995) 607-619. [https://doi.org/10.1016/0301-9322\(95\)00011-L](https://doi.org/10.1016/0301-9322(95)00011-L).
- [28] A.B. Biswas, S.K. Das, Two-phase frictional pressure drop of gas-non-Newtonian liquid flow through helical coils in vertical orientation, *Chem. Eng. Prog.* 47 (2008) 816–826. <https://doi.org/10.1016/j.cep.2007.01.030>
- [29] A.K. Thandlam, T.K. Mandal, S.K. Majumder, Flow pattern transition, frictional pressure drop, and holdup of gas non-Newtonian fluid flow in helical tube, *ASIA-Pacific J. Chem. Eng.* 10 (2015) 422–437. <https://doi.org/10.1002/apj.1886>.
- [30] G.D. Xia, X.F. Liu, An investigation of two-phase flow pressure drop in helical rectangular channel, *Int. Comm. Heat Mass Transfer.* 54 (2014) 33-41. <https://doi.org/10.1016/j.icheatmasstransfer.2014.03.009>.
- [31] X.F. Liu, G.D. Xia, G. Yang, Experimental study on the characteristics of air-water two-phase flow in vertical helical rectangular channel, *Int. J. Multiph. Flow.* 73 (2015) 227–237. <https://doi.org/10.1016/j.ijmultiphaseflow.2015.03.012>.
- [32] X.F. Liu, D.H. Zhao, Y.F. Liu, S. Jiang, H.Z. Xiang. Numerical analysis of the two-phase flow characteristics in vertical downward helical pipe[J]. *Int. J. Heat Mass Tran.* 108 (2017) 1947–1959. <https://doi.org/10.1016/j.ijheatmasstransfer.2017.01.056>
- [33] L. Cheng, G. Ribatski, L. Wojtan, J.R. Thome, New flow boiling heat transfer model and flow pattern map for carbon dioxide evaporation inside horizontal tubes, *Int. J. Heat Mass Transfer.* 49 (2006) 4082-4094. <https://doi.org/10.1016/j.ijheatmasstransfer.2006.04.003>

- [34] L. Cheng, G. Ribatski, J. Moreno Quibén, J.R. Thome, New prediction methods for CO₂ evaporation inside tubes: Part I - A two-phase flow pattern map and a flow pattern based phenomenological model for two-phase flow frictional pressure drops, *Int. J. Heat Mass Transfer*. 51 (2008) 111-124. <https://doi.org/10.1016/j.ijheatmasstransfer.2012.05.044>
- [35] J.R. Taylor, *An Introduction to Error Analysis*, second ed., University Science Books, 1982. <https://doi.org/10.1119/1.13309>
- [36] B. Cai, G.D. Xia, L. Cheng, Z.P. Wang, Flow regime visualization and identification of air-water two-phase flow in a horizontal helically coiled rectangular channel, *Heat Transfer Eng.* 43 (2022) 720-736. <https://doi.org/10.1080/01457632.2021.1905313>.
- [37] G.D. Xia, B. Cai, L. Cheng, Z.P. Wang, Y.T. Jia, Experimental study and modelling of average void fraction of gas-liquid two-phase flow in a helically coiled rectangular channel, *Exp. Therm. Fluid Sci.* 94 (2018) 9–22. <https://doi.org/10.1016/j.expthermflusci.2018.01.027>.

List of table captions

Table 1. Geometry parameters of the helical coiled rectangular tube.

Table 2. Experimental conditions.

Table 3. Uncertainties of the measured parameters in the experiments.

Table 4. Single phase friction pressure correlations in coiled tubes.

Table 5. The values of parameter C .

Table 1. Geometry parameters of the helical rectangular tube.

Parameters	Value
Channel height, h (m)	0.034
Channel width, w (m)	0.025
Pitch, P (m)	0.140
Coil diameter, D (m)	0.141
Helix angle, φ (rad)	0.306

Table 2. Experimental conditions.

Fluids	Superficial velocity (m/s)
Air	0.13 - 16
Water	0.11 - 2

Table 3. Uncertainties of the measured parameters in the experiments.

Measurement parameters	Uncertainty
Channel width, w (m)	$\pm 2\%$
Channel height, h (m)	$\pm 1.47\%$
Area of channel, A (m ²)	$\pm 3.47\%$
Liquid volumetric flow rate, Q_L (m ³ /s)	$\pm 1.5\%$
Gas volumetric flow rate, Q_G (m ³ /s)	$\pm 0.5\%$
Liquid phase superficial velocity, U_{SL} (m/s)	$\pm 4.97\%$
Gas phase superficial velocity, U_{SG} (m/s)	$\pm 3.97\%$
Time-averaged local void fraction, $\alpha(y)$	$\pm 8.65\%$

Table 4. Single phase friction pressure correlations in coiled tubes.

Literature	Correlations
Laminar flow	
Ito [18]	$\frac{\lambda}{\lambda_s} = 0.1033Dn^{0.5} \left[\left(1 + \frac{1.729}{Dn} \right)^{0.5} - \left(\frac{1.729}{Dn} \right)^{0.5} \right]^{-3}, \quad \lambda_s = 64/Re$
Manlapaz et. al [20]	$\frac{\lambda}{\lambda_s} = \left[\left(1.0 - \frac{0.18}{\left[1 + (35/Dn)^2 \right]^{0.5}} \right)^r + \left(1 + \frac{d/D}{3} \right)^2 \left(\frac{Dn}{88.33} \right) \right]^{2.5},$ $\lambda_s = 64/Re$ $Dn < 20, r = 2; 20 < Dn < 40, r = 1; Dn > 40, r = 0$
White [21]	$\frac{\lambda}{\lambda_s} = \frac{1}{1 - \left[1 - (11.6/Dn)^{0.45} \right]^{(1/0.45)}}, \quad \lambda_s = 64/Re$
Turbulent flow	
Ito [19]	$\lambda = 0.304Re_L^{-0.25} + 0.029 \left(\frac{d_h}{D} \right)^{0.5}$
Srinivasan et. al [22]	$\lambda = 0.336Re_L^{-0.2} (d_h/D)^{0.1}, \quad Re (d/D)^{0.5} \leq 14000$
Ali [23]	$\lambda = 0.18Re_L^{-1/8} (d_h/D_{eq})^{0.15}, \quad D_{eq} = \sqrt{P^2 + (\pi D)^2} / \pi$

Table 5 The values of parameter C .

laminar-laminar(ll)	laminar -turbulent(lt)	turbulent – laminar(tl)	turbulent – turbulent(tt)
20	12	10	5

List of figure captions

Fig. 1. Schematic diagram of the experimental setup of air-water two-phase flow in the helically coiled rectangular tube.

Fig. 2. Schematic diagram of the horizontal helically coiled rectangular tube and its geometry dimensions.

Fig. 3. (a) Illustration of the 13 measurement positions of the electric conductivity probes in the rectangular channel; (b) Structure of the electric conductivity probe used in the measurement of the local void fraction and spatial phase distribution.

Fig. 4. The output signal of the electric conductivity probe and its transformation into the square wave.

Fig. 5. Comparison of the resident times of the slug units measured with the electric conductivity probe method with the visualization method for the Taylor bubbles and liquid slugs at $U_{SG} = 4.346$ m/s and $U_{SL} = 0.605$ m/s.

Fig. 6. Variation of the local void fractions for three gas superficial velocities at a fixed liquid superficial velocity in the severe slugging flow regime.

Fig. 7. Variation of the local void fractions for three liquid superficial velocities at a fixed gas superficial velocity in the severe slugging flow regime.

Fig. 8. The local void fraction distributions in the bubbly flow regime for three gas superficial velocities at a fixed liquid superficial velocity.

Fig. 9. The local void fraction distributions in the bubbly flow regime for three liquid superficial velocities at a fixed gas superficial velocity.

Fig. 10 Two phase flow regime images at various superficial gas and liquid velocities in the coiled rectangular tube.

Fig. 11. The local void fraction distributions in the intermittent flow regime for three gas superficial velocities at a fixed liquid superficial velocity.

Fig. 12. The local void fraction distributions in the intermittent flow regime for three liquid superficial velocities at a fixed gas superficial velocity.

Fig. 13. The local void fraction distributions in the annular flow regime for three gas superficial velocities at a fixed liquid superficial velocity.

Fig. 14. The local void fraction distributions in the annular flow regime for three liquid superficial velocities at a fixed gas superficial velocity.

Fig. 15. Experimental and fitted local void fraction distribution profiles at four positions along the flow direction for $U_{SG} = 1.21$ m/s (a) $U_{SL} = 0.6$ m/s; (b) $U_{SL} = 0.8$ m/s.

Fig. 16. Variation of single-phase liquid flow friction coefficient versus the Reynolds number in the spirally coiled rectangular tube. (1) Ito [18]; (2) Manlapaz et al. [20]; (3) White [21]; (4) Ito [19]; (5) Srinivansan et al. [22]; (6) Ali [23].

Fig.17. Comparison of the experimental single-phase flow friction coefficients to the predicted results with the proposed correlation Eq. (10).

Fig. 18. Effect of superficial liquid and gas flow velocities on the two phase frictional pressure drop.

Fig.19. Effect of flow regimes on the two phase frictional pressure drops at different superficial gas velocities.

Fig.20. Variation of the liquid phase two phase multiplier Φ_L with the L-M parameter X . (L-M correlation [6]).

Fig. 21. Comparison of the experimental two phase flow liquid phase multipliers Φ_L to the prediction results with the Awwad et al. correlation [27].

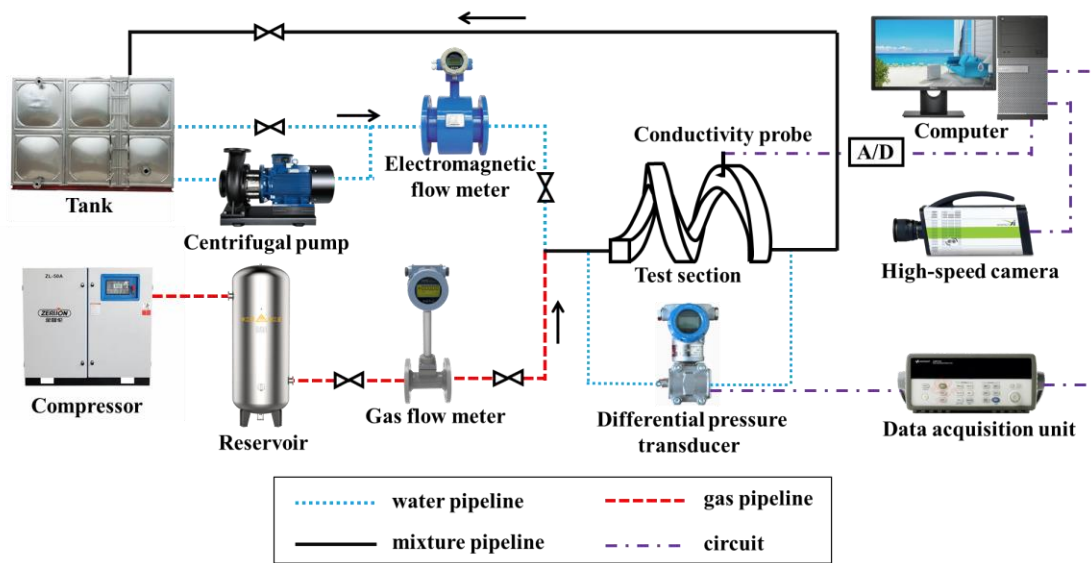


Fig. 1. Schematic diagram of the experimental setup of air-water two-phase flow in the helically coiled rectangular tube.

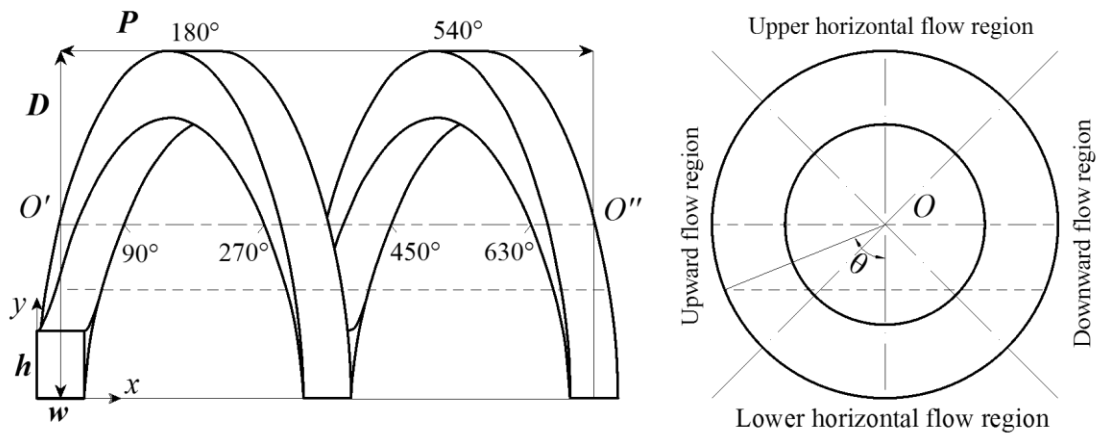


Fig. 2. Schematic diagram of the horizontal helically coiled rectangular tube and its geometry dimensions.

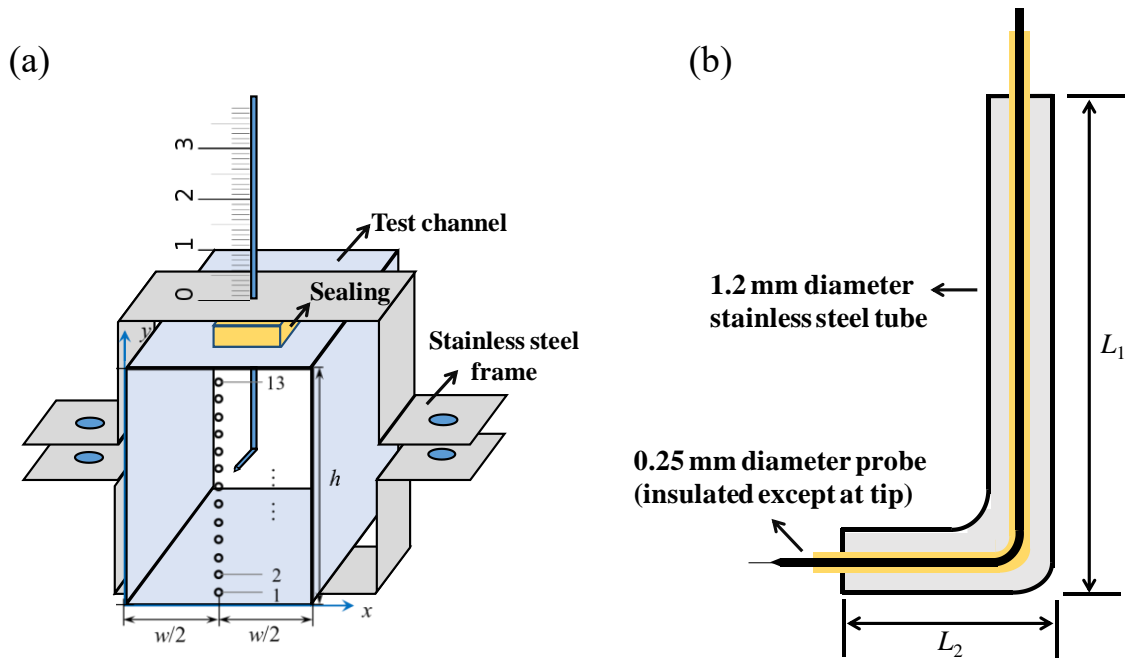


Fig. 3. (a) Illustration of the 13 measurement positions of the electric conductivity probes in the rectangular channel; (b) Structure of the electric conductivity probe used in the measurement of the local void fraction and spatial phase distribution.

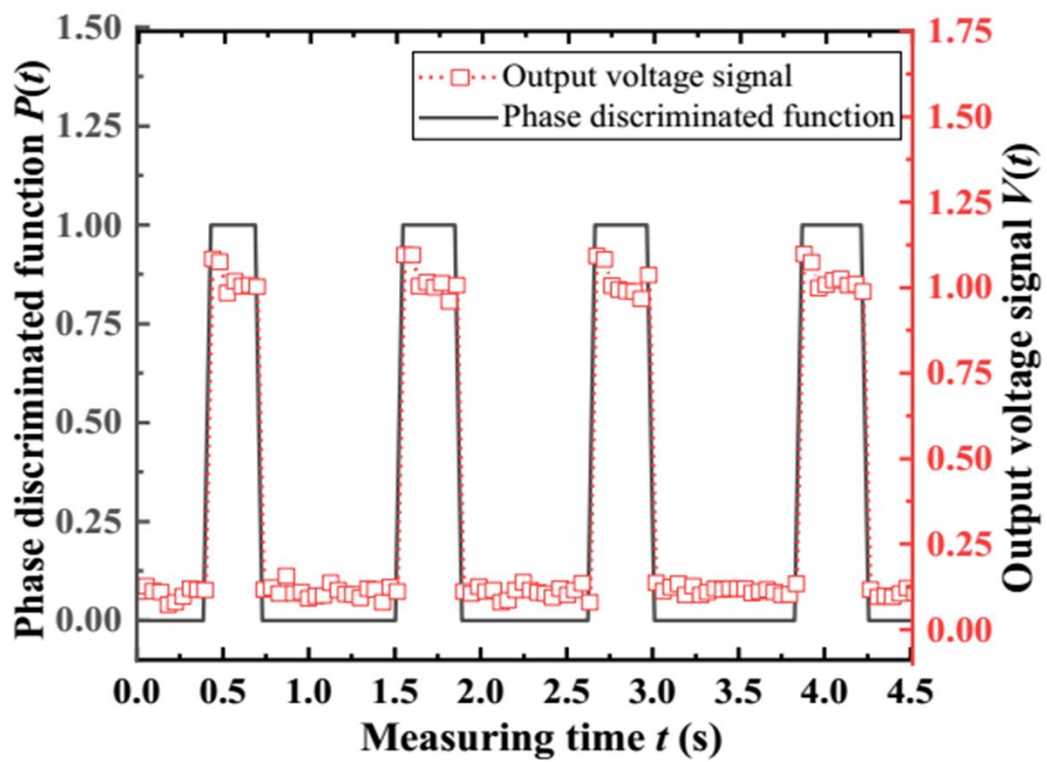


Fig. 4. The output signal of the electric conductivity probe and its transformation into the square wave.

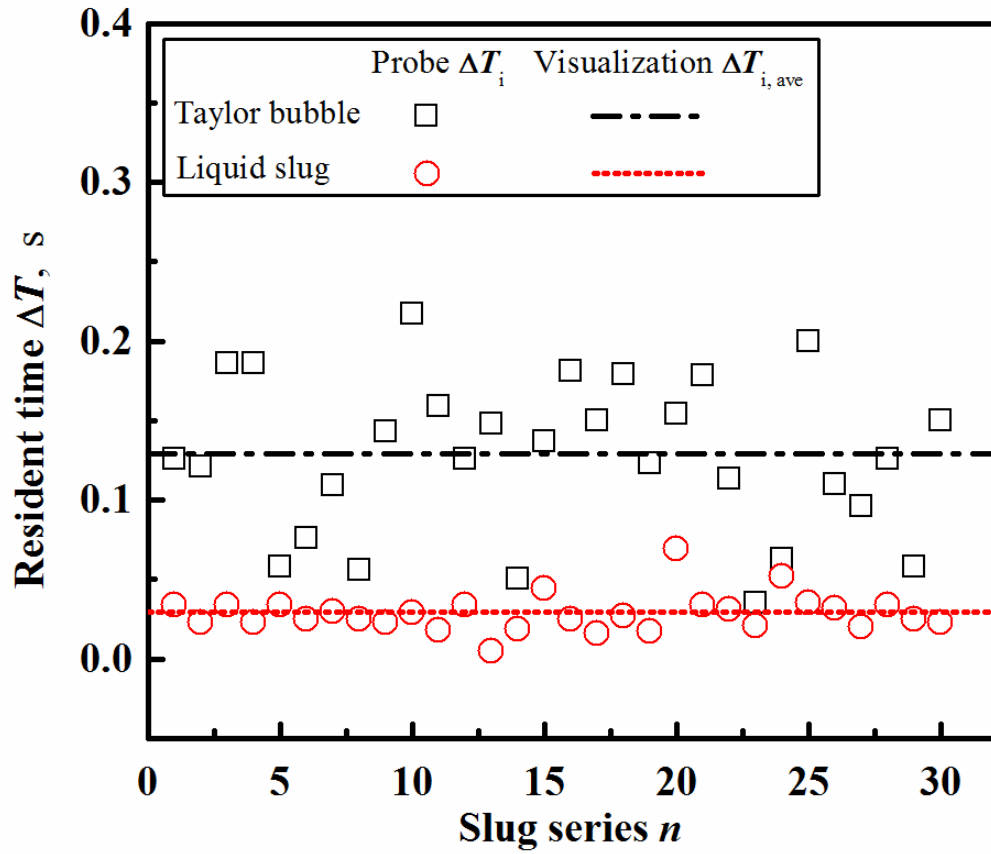


Fig. 5. Comparison of the resident times of the slug units measured with the electric conductivity probe method with the visualization method for the Taylor bubbles and liquid slugs at $U_{SG} = 4.346$ m/s and $U_{SL} = 0.605$ m/s.

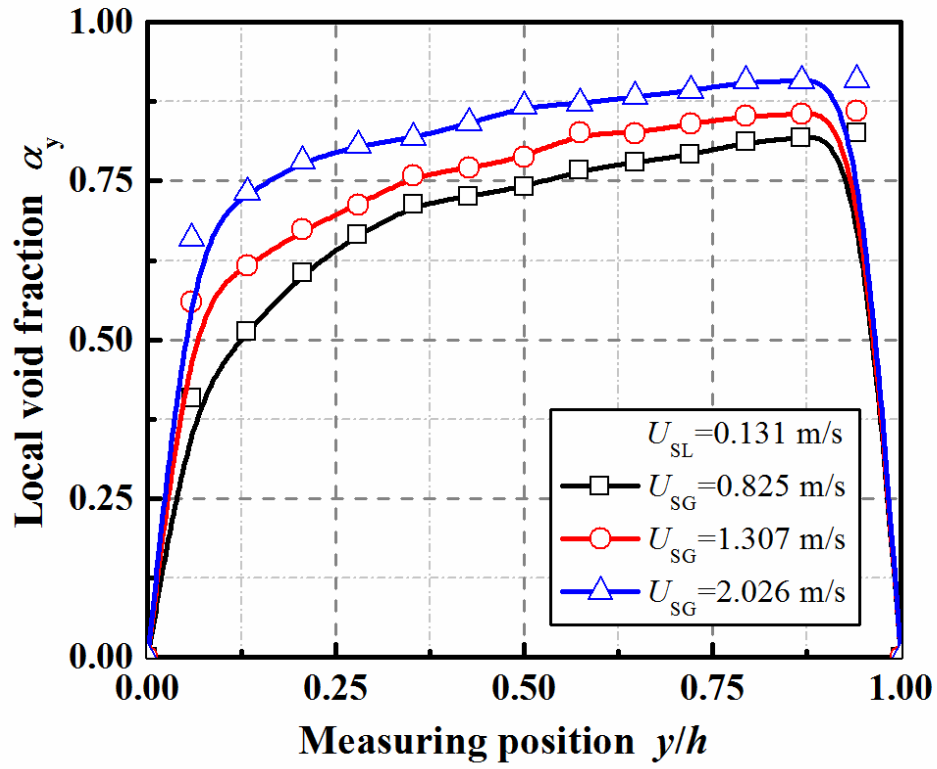


Fig. 6. Variation of the local void fractions for three gas superficial velocities at a fixed liquid superficial velocity in the severe slugging flow regime.

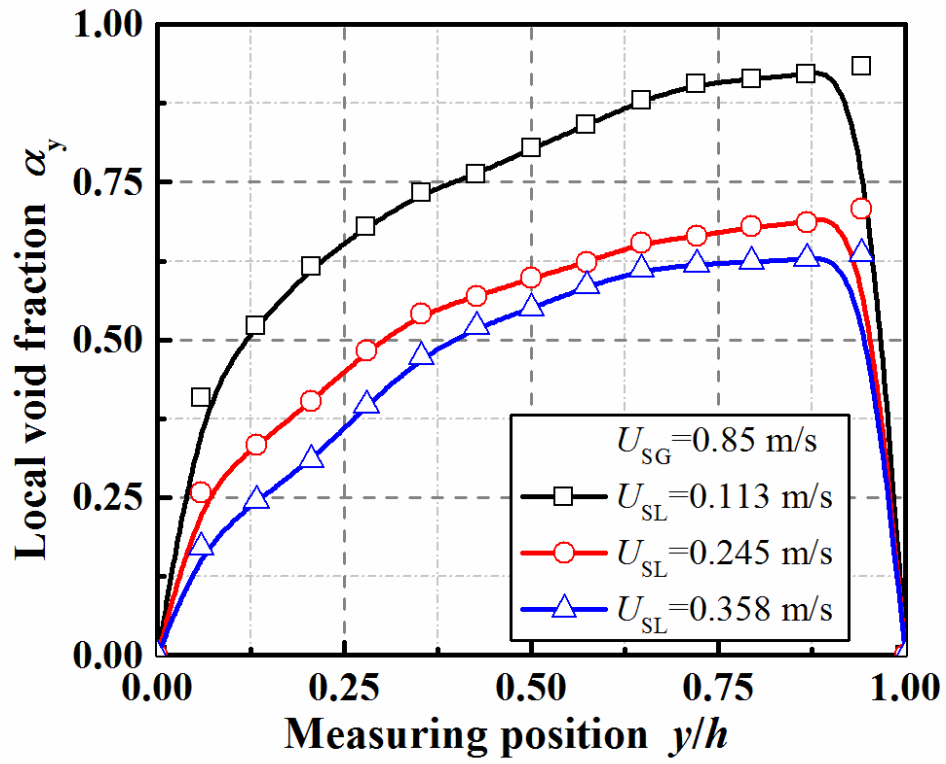


Fig. 7. Variation of the local void fractions for three liquid superficial velocities at a fixed gas superficial velocity in the severe slugging flow regime.

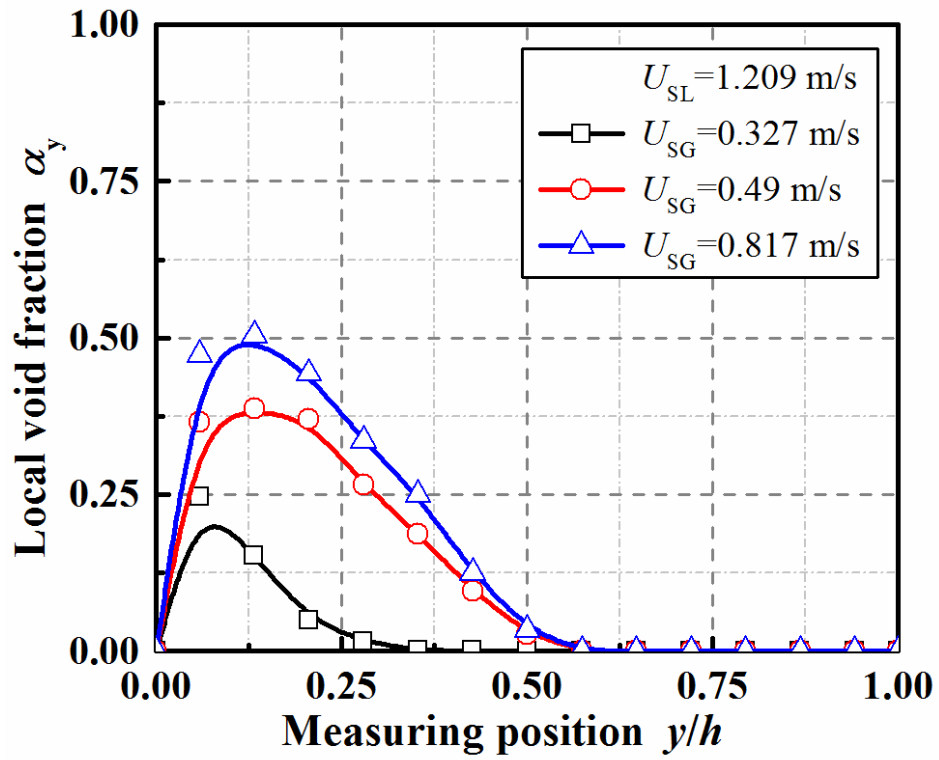


Fig. 8. The local void fraction distributions in the bubbly flow regime for three gas superficial velocities at a fixed liquid superficial velocity.

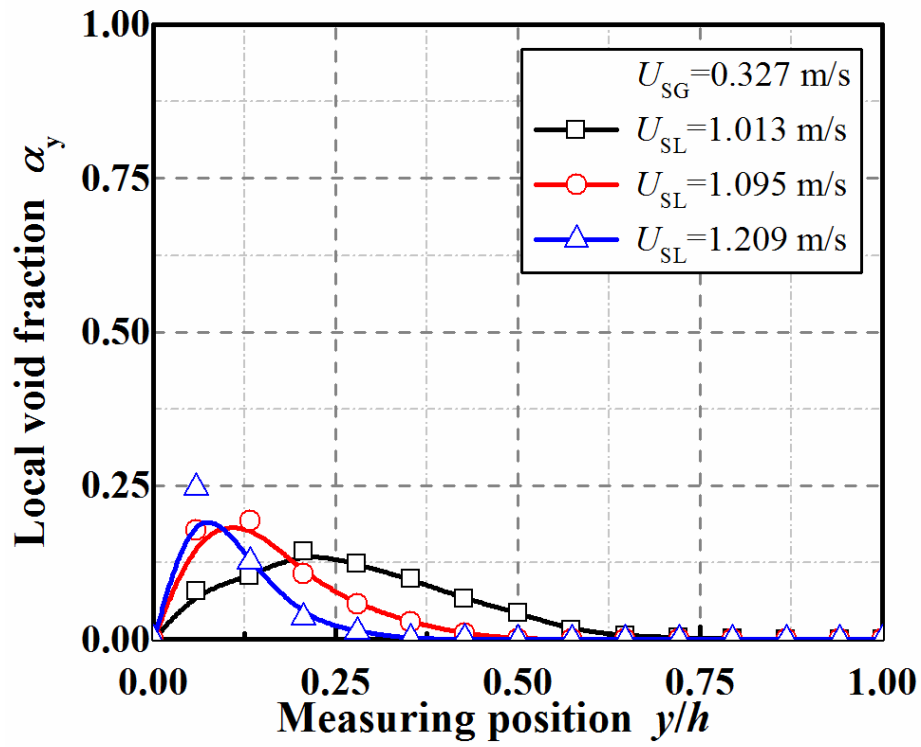


Fig. 9. The local void fraction distributions in the bubbly flow regime for three liquid superficial velocities at a fixed gas superficial velocity.

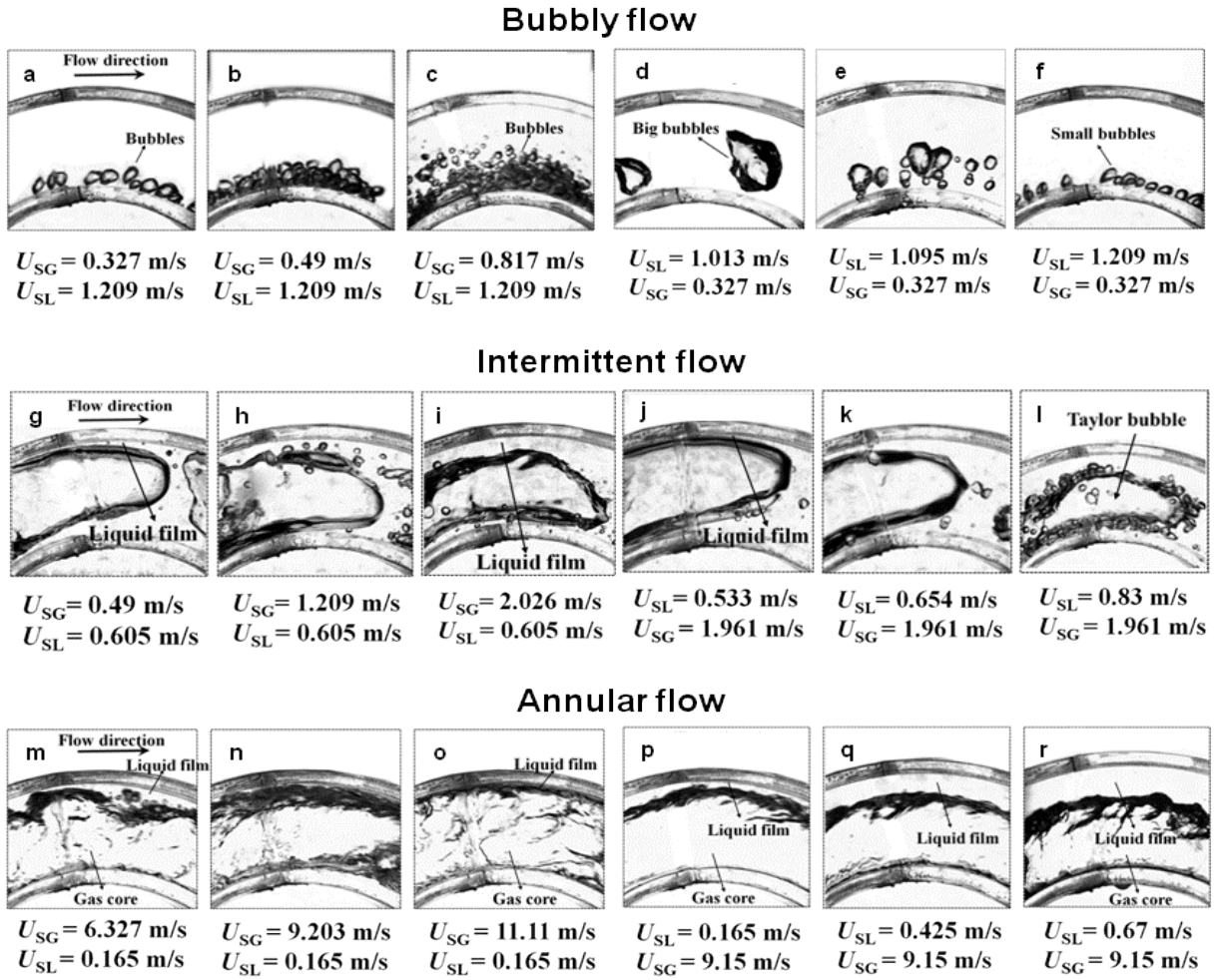


Fig. 10 Two phase flow regime images at various superficial gas and liquid velocities in the coiled rectangular tube.

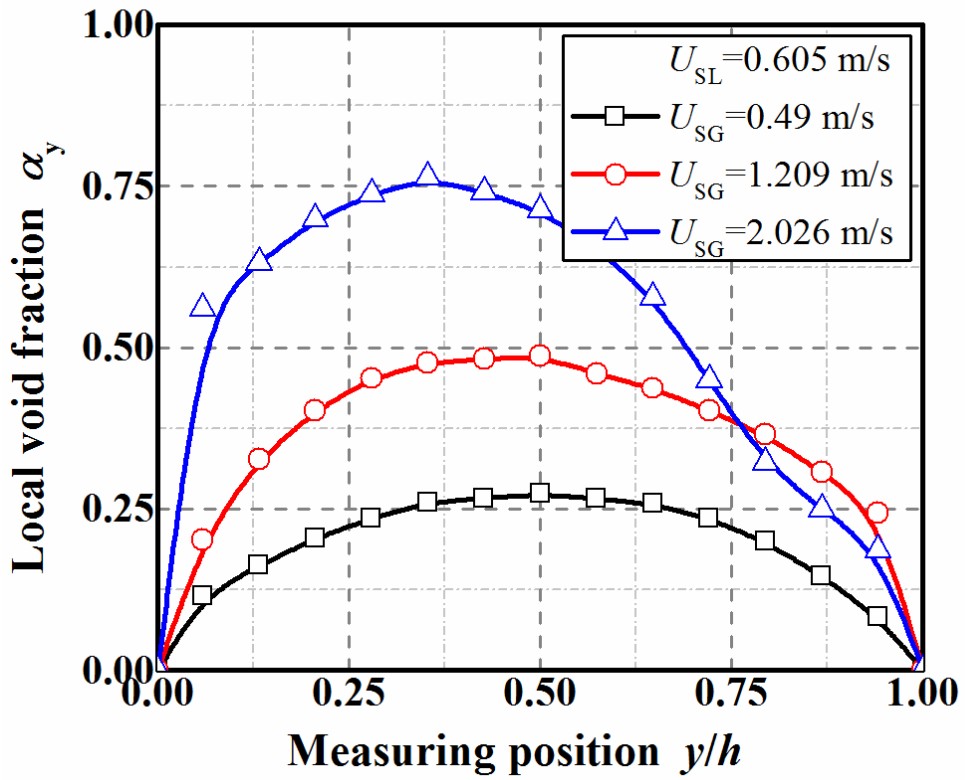


Fig. 11. The local void fraction distributions in the intermittent flow regime for three gas superficial velocities at a fixed liquid superficial velocity.

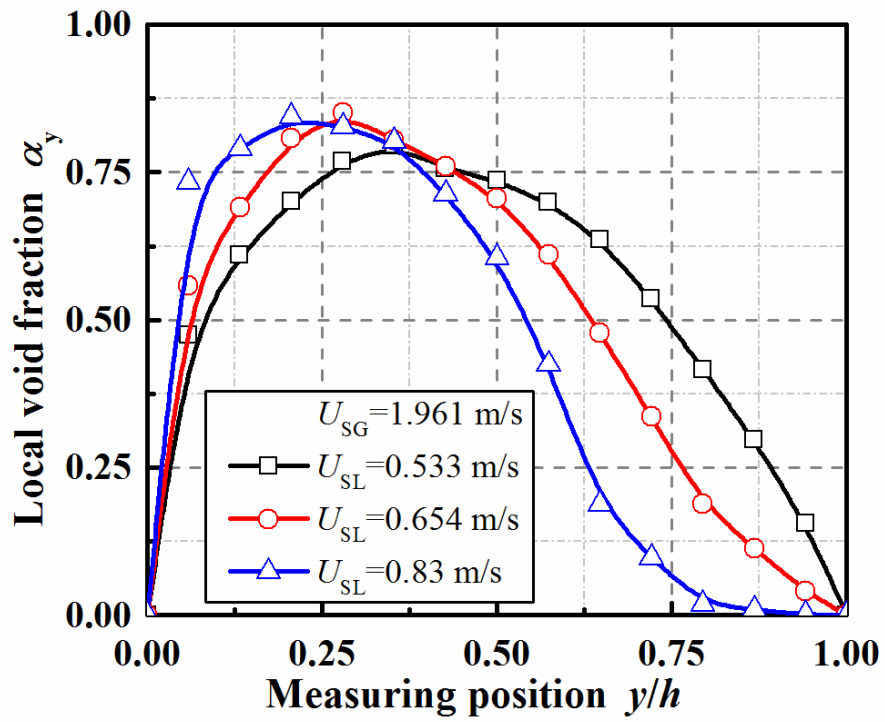


Fig. 12. The local void fraction distributions in the intermittent flow regime for three liquid superficial velocities at a fixed gas superficial velocity.

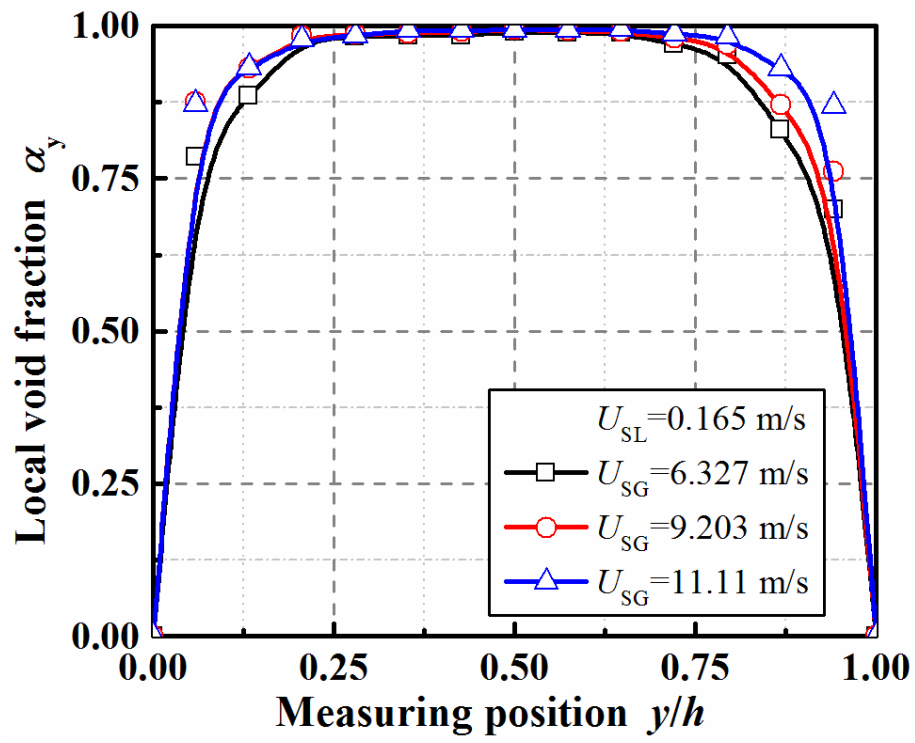


Fig. 13. The local void fraction distributions in the annular flow regime for three gas superficial velocities at a fixed liquid superficial velocity.

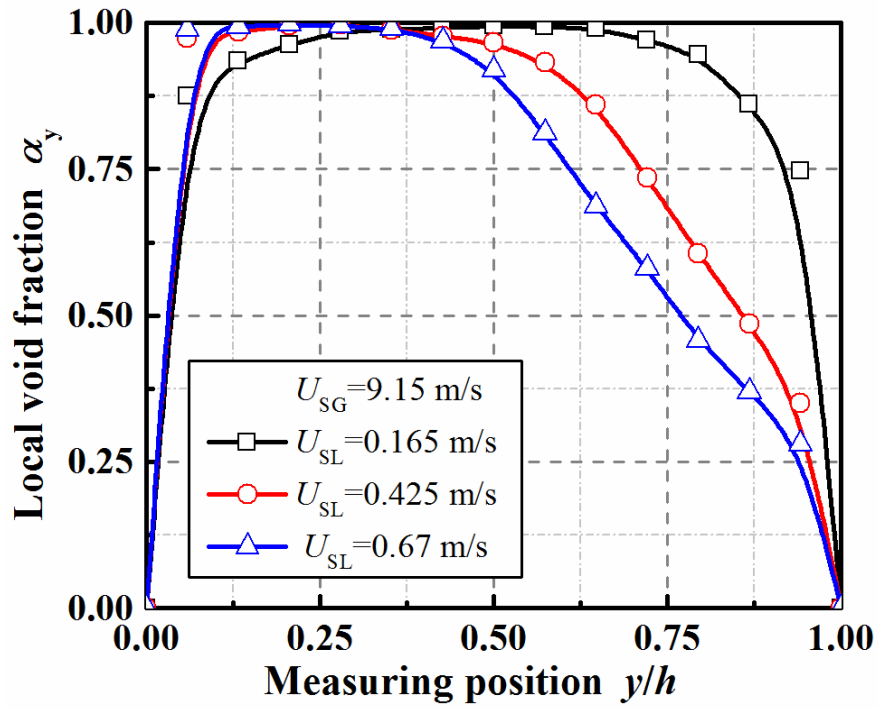


Fig. 14. The local void fraction distributions in the annular flow regime for three liquid superficial velocities at a fixed gas superficial velocity.

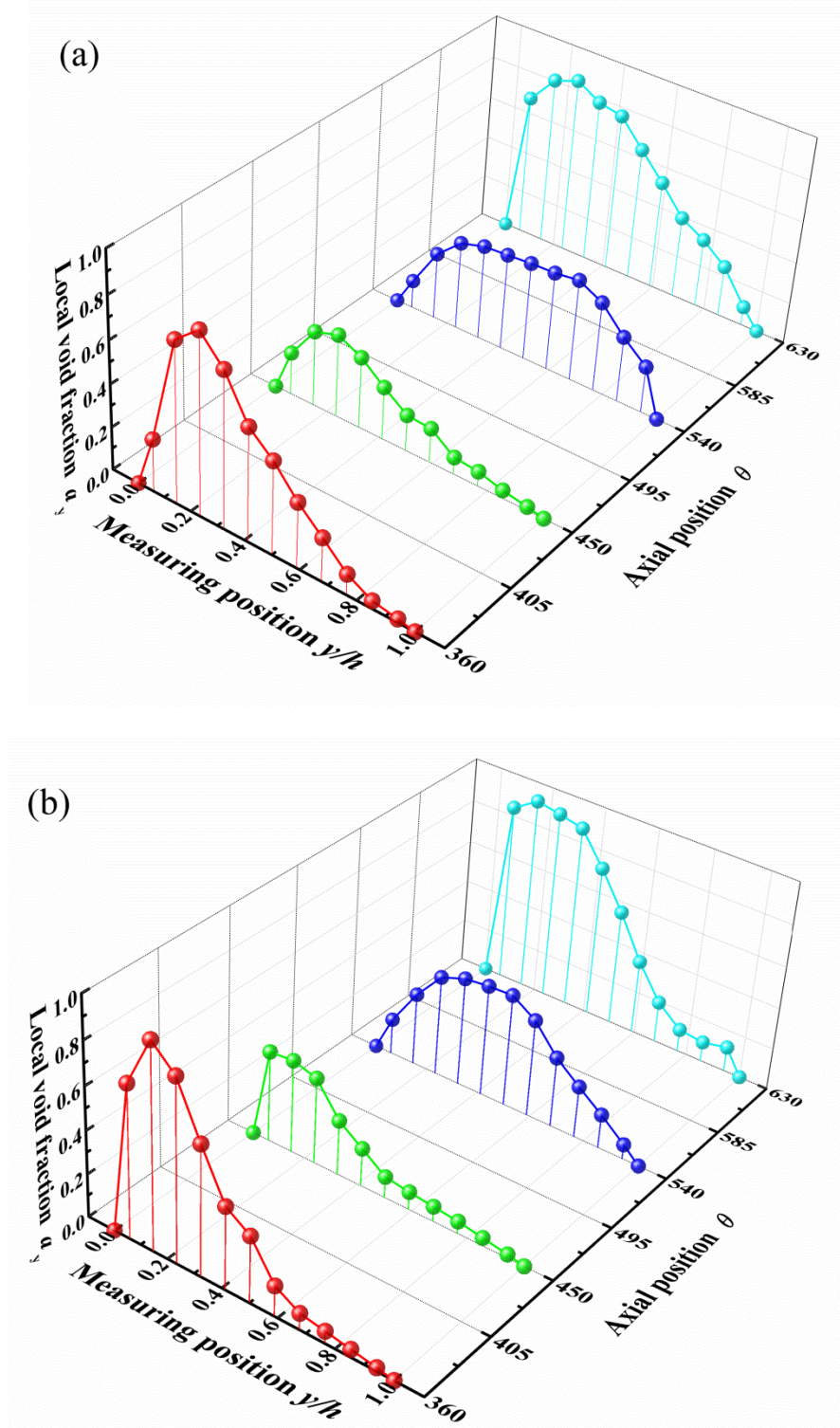


Fig. 15. Experimental and fitted local void fraction distribution profiles at four positions along the flow direction for $U_{SG} = 1.21$ m/s (a) $U_{SL} = 0.6$ m/s; (b) $U_{SL} = 0.8$ m/s.

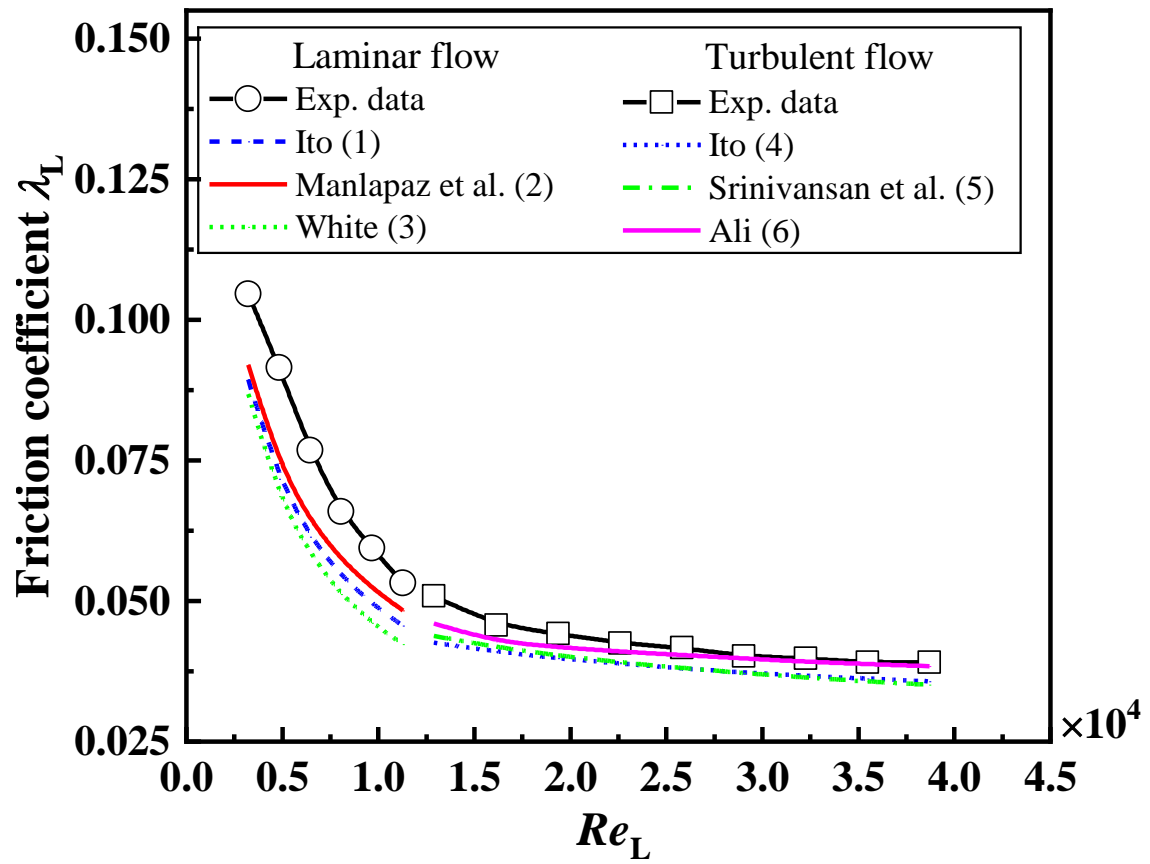


Fig. 16. Variation of single-phase liquid flow friction coefficient versus the Reynolds number in the spirally coiled rectangular tube: (1) [18], (2) [20], (3) [21], (4) [19], (5) [22] and (6) [23].

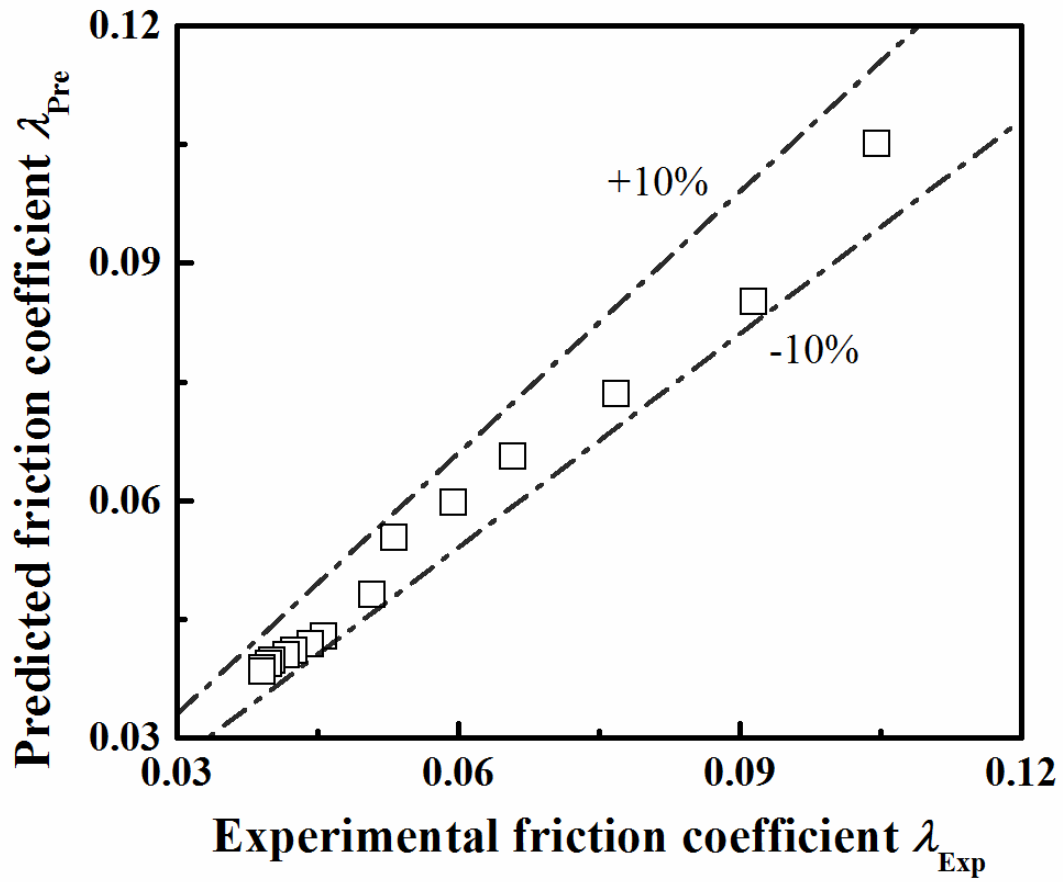


Fig.17. Comparison of the experimental single-phase flow friction coefficients to the predicted results with the proposed correlation Eq. (9).

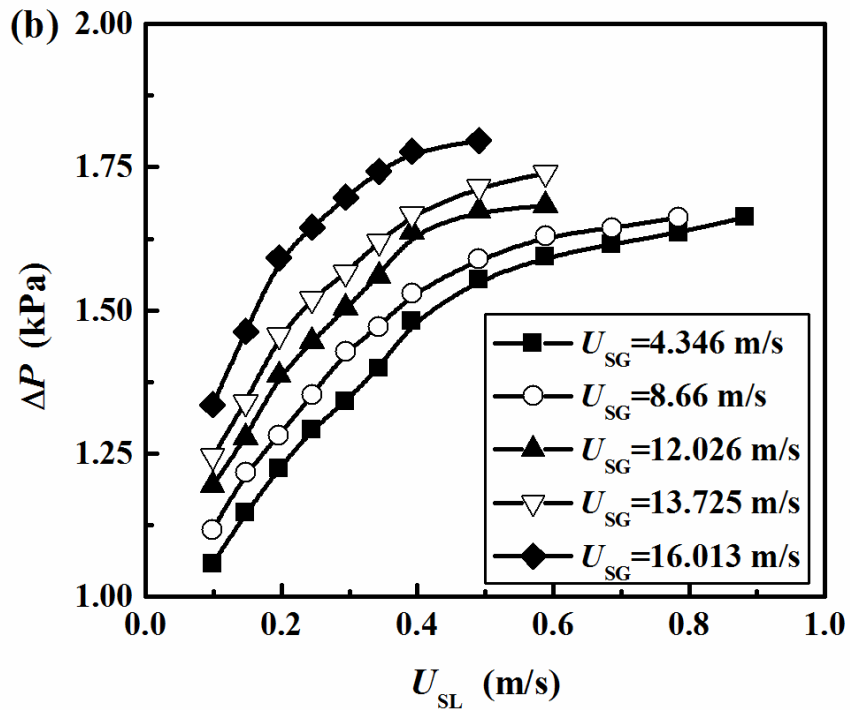
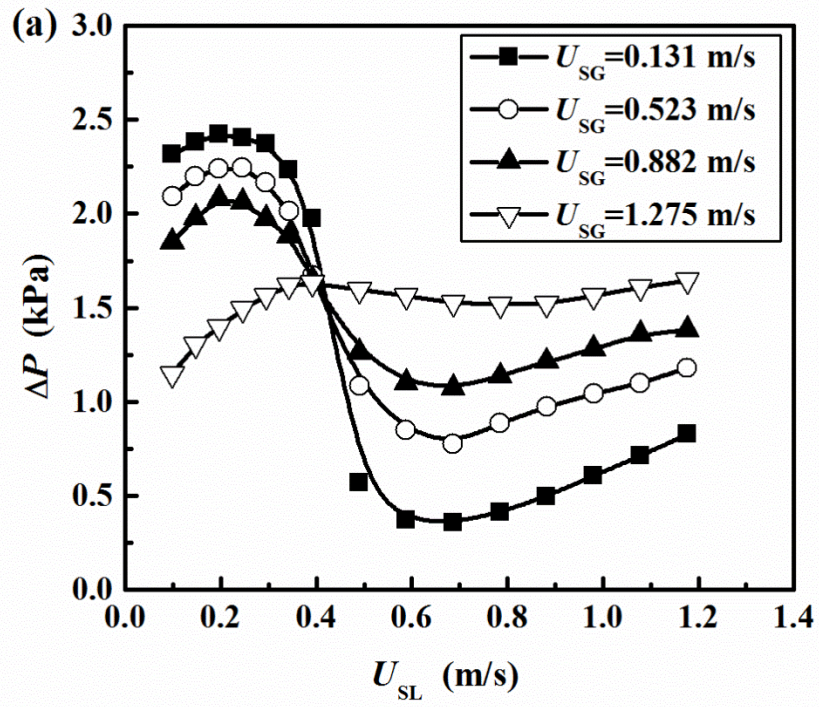


Fig. 18. Effect of the superficial liquid and gas flow velocities on the two phase frictional pressure drops.

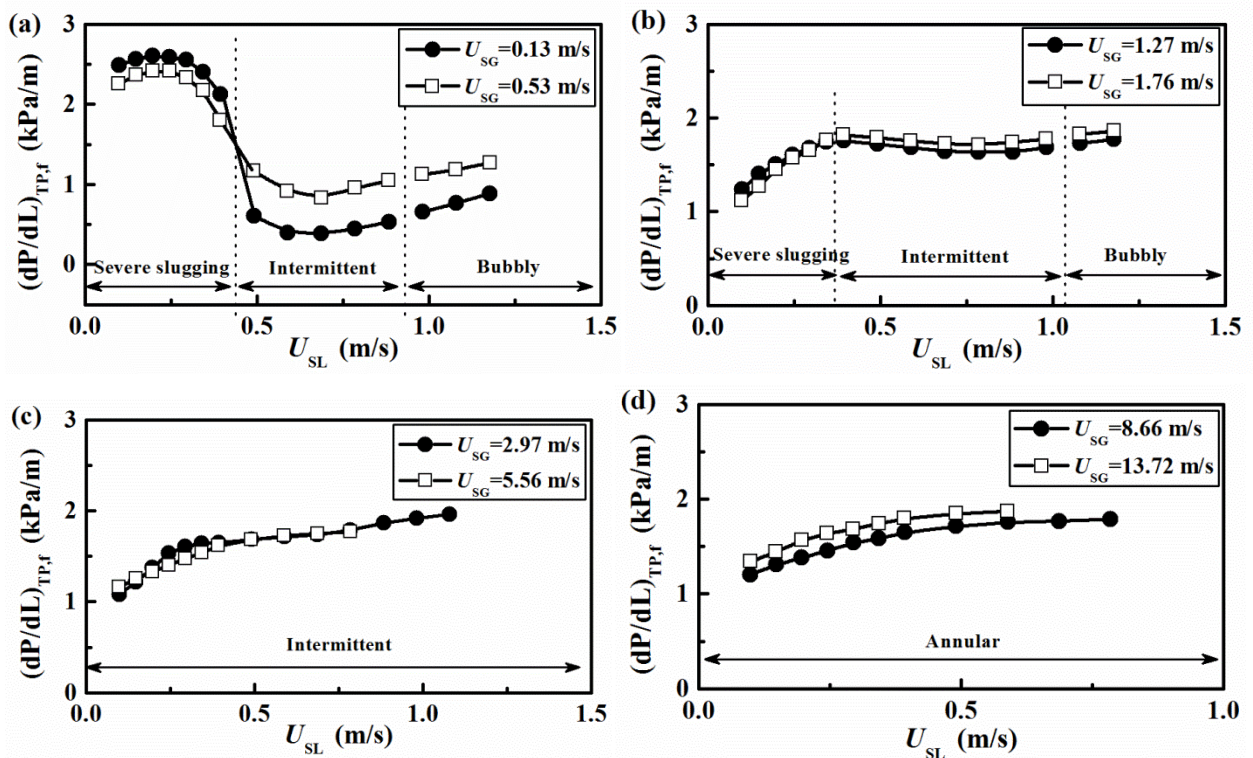


Fig.19. Effect of flow regimes on the two phase frictional pressure drops at different superficial gas velocities.

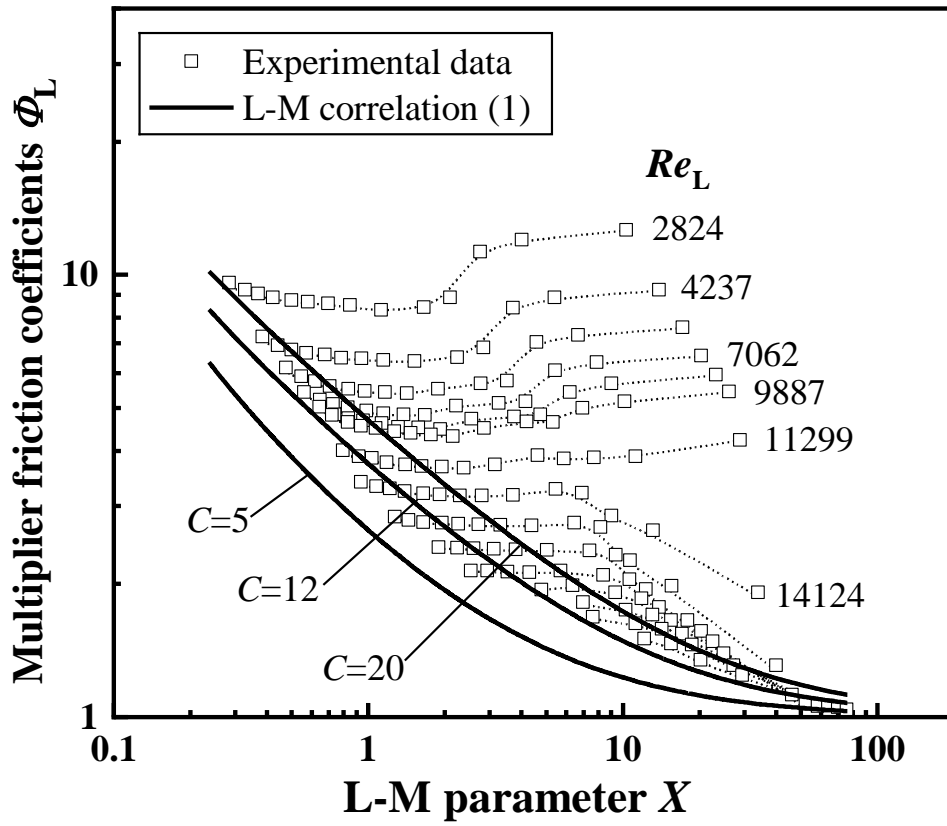


Fig. 20. Variation of liquid phase two phase multiplier Φ_L with the Martinelli number X . (L-M correlation [6]).

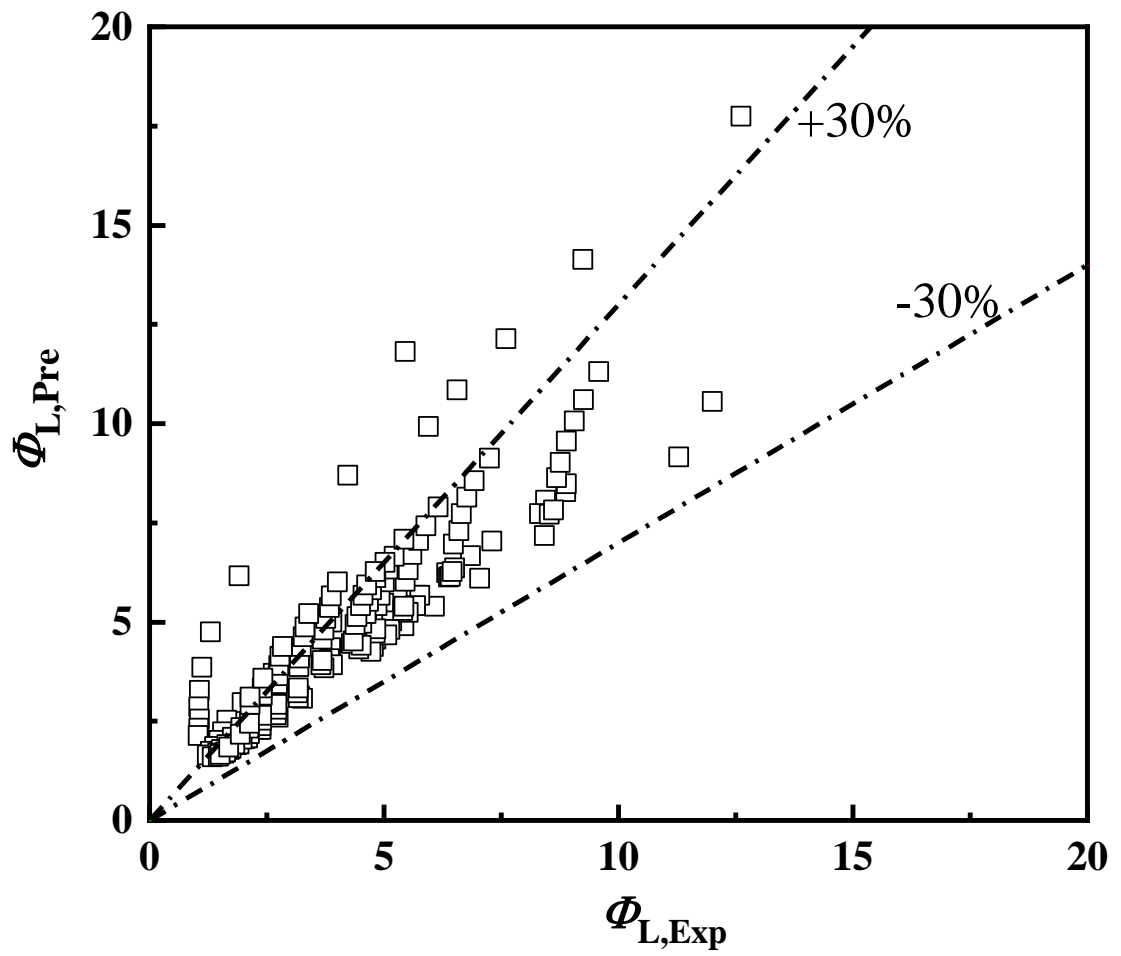


Fig. 21. Comparison of the experimental two phase flow liquid phase multipliers Φ_L to the prediction results with the Awwad et al. correlation [27].